Biogeosciences Discuss., https://doi.org/10.5194/bg-2018-408
Manuscript under review for journal Biogeosciences
Discussion started: 12 October 2018

Biogeosciences Discussions Open Access EGU

Seasonal Net Ecosystem Metabolism of the Near-Shore Reef System in La Parguera, Puerto Rico

Melissa Meléndez[1]
Joseph Salisbury[1]
Dwight Gledhill[2]
Chris Langdon[3]
Julio M. Morell[4,5]
Derek Manzello[6]
Sylvia Musielewicz[7,8]
Adrienne Sutton[7]

Affiliation and address

[1]Department of Earth Sciences and Ocean Processes Analysis Laboratory, University of New Hampshire, Durham, New Hampshire, 03824, USA
[2]National Oceanic and Atmospheric Administration (NOAA), Ocean Acidification Program, Silver Spring, Maryland, 20910, USA
[3]Rosenstiel School of Marine and Atmospheric Science, University of Miami, Miami, FL, USA
[4]Department of Marine Sciences, University of Puerto Rico, Mayagüez, Puerto Rico, 00680, USA
[5]Caribbean Coastal Ocean Observing System, NOAA, Magueyes Island, Lajas, Puerto Rico, 00667, USA
[6]Atlantic Oceanographic and Meteorological Laboratory, NOAA, Miami, Florida, USA
[7]Pacific Marine Environmental Laboratory, NOAA, Seattle, Washington, 98115, USA
[8]University of Washington Joint Institute for the Study of the Atmosphere and Ocean, Seattle, WA 98195, USA

Correspondence to: Melissa Meléndez (mm19@wildcats.unh.edu)

Keywords: Puerto Rico, Coral Reef, Net Ecosystem Calcification, Net Ecosystem Production, Dissolution, Carbonate Chemistry

Biogeosciences Discuss., https://doi.org/10.5194/bg-2018-408
Manuscript under review for journal Biogeosciences
Discussion started: 12 October 2018

Abstract

Changes in ocean chemistry as a direct response to rising atmospheric carbon dioxide (CO_2) concentrations is causing a reduction of pH in the surface ocean. While the dynamics and trends in carbonate chemistry are reasonably constrained for open ocean waters, the ways in which ocean acidification (OA) manifests within the shallow near-shore waters, where coral reefs reside, is less understood. Constraining near-reef variability in carbonate chemistry and net ecosystem metabolic processes across diel, seasonal, and annual scales is important in evaluating potential biogeochemical thresholds of OA that could result in ecological community changes. The OA Test-Bed at La Parguera Marine Reserve in Puerto Rico provides long-term carbonate chemistry observations at high-temporal resolution within a Caribbean near-shore coral reef ecosystem. A 1-D model was developed using the carbon mass balance approach to yield information about net ecosystem production and calcification processes occurring in the water column adjacent to the reef. We present results of nine years of sustained monitoring at the Enrique mid-shelf forereef, which provides for the characterization of temporal dynamics in carbonate chemistry and net ecosystem metabolic processes encompassing near-shore and upstream locations. Results indicate that net heterotrophy and net dissolution dominate over most of the year, while net autotrophic conditions coupled with calcification dominated from only January to mid-April. The average carbonate dissolution rate observed during summer is estimated at -2.19 g $CaCO_3$ m^{-2} day^{-1} and net community dissolution persists 76 % of the seasonal year despite the water column remaining super-saturated with respect to aragonite. This corresponds to -0.62 kg $CaCO_3$ m^{-2} $year^{-1}$, classifying the Enrique fore-reef and off-reef areas in a net dissolutional state. The combination of thermodynamically-driven depressed aragonite saturation state and high rates of respiration during the summer cause conditions that jeopardize the most soluble carbonate minerals and the free energy in the system for calcification. These data suggest that the reef area and associated ecosystems upstream of the sampling location are experiencing a net loss of $CaCO_3$, possibly compromising coral ecosystem health and reef accretion processes necessary for maintenance as sea level increases. Resiliency from other climate-scale stressors including rising sea surface temperatures and coral bleaching is likely to be compromised in a system exhibiting net carbonate loss.

Biogeosciences Discuss., https://doi.org/10.5194/bg-2018-408
Manuscript under review for journal Biogeosciences
Discussion started: 12 October 2018

1 Introduction

Oceans are the largest natural sink for excess atmospheric carbon dioxide ($CO_{2,air}$), currently absorbing approximately one-third (~ 28 %) of all anthropogenic $CO_{2,air}$ each year (Sabine et al., 2004; Le Quéré et al., 2016). Under CO_2 "baseline scenarios" of the Intergovernmental Panel on Climate Change (IPCC) Representative Concentration Pathways (RCP6.0 and RCP8.5), dissolved CO_2 in the surface ocean ($CO_{2,sw}$) will likely double over its pre-industrial concentration (~280 µatm) by the middle of this century, producing significant changes in the ocean carbonate chemistry (IPCC, 2014).

As $CO_{2,air}$ is absorbed by the surface ocean it reacts to form carbonic acid (H_2CO_3) which rapidly dissociates to hydrogen ion (H^+) and bicarbonate ion (HCO_3^-), thereby lowering pH and hence the term "acidification". The resulting change in pH is buffered in part by the reaction of H^+ with carbonate ions (CO_3^{2-}) forming bicarbonate. The low pH favors bicarbonate over carbonate thereby driving a net depletion of carbonate ions, as given by:

$$CO_{2,air} \leftrightarrow CO_{2,sw} + H_2O \leftrightarrow \underbrace{H_2CO_3}_{Carbonic\ Acid} \leftrightarrow H^+ + \underbrace{HCO_3^-}_{Bicarbonate} \leftrightarrow 2H^+ + \underbrace{CO_3^{2-}}_{Carbonate} \quad (1)$$

This chemical process affects the degree to which seawater is saturated with respect to calcium carbonate ($CaCO_3$) minerals:

$$Ca^{2+} + CO_3^{2-} \leftrightarrow CaCO_{3,solid} \quad (2)$$

where, Ca^{2+} is the calcium ion. The solubility of $CaCO_3$ minerals in seawater is described by Mucci (1983) and is defined according to the stoichiometric solubility product constant (K^*_{SP}) as a function of temperature, pressure, and solution composition. The degree of carbonate saturation with respect to the $CaCO_3$ mineral phase of interest (e.g., calcite, aragonite, Mg-calcite) is indicated by the saturation state (Ω). Aragonite and calcite represent the most important calcium carbonate polymorphs, but Mg-calcite can contain variable amounts of magnesium ion (Mg^{2+}) ranging from 10 to >30% (Morse et al., 2007).

Biogeosciences Discuss., https://doi.org/10.5194/bg-2018-408
Manuscript under review for journal Biogeosciences
Discussion started: 12 October 2018

87 The Ω is defined as the ratio of concentration product to K^*_{SP}:

88

89 $$\Omega_x = \frac{[Ca^{2+}]\,[Mg^{2+}][CO_3^{2-}]}{K^*_{sp}} \quad (3)$$

90

91 where, [ ] indicates total concentrations. Values of $\Omega > 1$ are typical for tropical surface ocean waters and
92 indicate that precipitation of the mineral phase is favored; if $\Omega < 1$ dissolution is favored; and if $\Omega = 1$ the
93 mineral is in equilibrium with seawater and no net dissolution nor precipitation is expected. The energy
94 available in the system to drive mineral precipitation can be related to Ω according to:

95

96 $$\Delta G = RT\ln\Omega_x = RT\ln\frac{IAP}{k_x} \quad (4)$$

97

98 where, ΔG is the Gibbs free energy (cal mol^{-1} $CaCO_3$), R is the ideal gas constant (J mol^{-1} K^{-1}), T is
99 absolute temperature (K), IAP is the ion activity product, and k is the thermodynamic solubility product.
100 The subscript x denotes the mineral phase of interest. While regions of the Southern Ocean surface waters
101 could experience under-saturation with respect to aragonite (i.e., $\Omega_{arag} < 1$), should $CO_{2,air}$ levels exceed
102 500 µatm, tropical surface oceanic waters are projected to remain supersaturated (i.e., $\Omega_{arag} > 1$) for several
103 centuries (Cao and Caldeira, 2008). Despite this continued super-saturation, concerns remain regarding
104 the energy required by calcifers to sustain calcification and the free energy available in the system to drive
105 mineral precipitation with continued OA (Cohen and Holcomb, 2009).

106

107 Multiple laboratory studies have reported reduced rates of calcification for many species of reef-building
108 coral as a function of changes in carbonate chemistry and Ω_{arag} (e.g., Borowitzka 1981; Gao et al., 1993;
109 Gattuso et al., 1998; Langdon et al., 2000, 2003; Leclercq et al., 2000, 2002; Marubini et al., 2001;
110 Marshall and Clode, 2002; Ohde and Hossain, 2004; Langdon and Atkinson, 2005; Anthony et al., 2008;
111 Chan and Connolly, 2013). The rates of calcification (carbonate production) respond negatively, while
112 biologically-mediated and metabolic dissolution respond positively to declining Ω_{arag}, representing not a
113 "switch" (i.e., threshold effect) response, but rather a "dimmer" effect (Andersson and Gledhill, 2013).

Experimental studies have also revealed that Ω_{arag} has an indirect effect on coral recruitment by disrupting larval-algal settlement interactions (Doropoulos et al., 2012) and direct effects on recruitment (Albright et al., 2010) which could prove far more disruptive under the combination of warming and elevated seawater CO_2 than under either stressor singly (Albright and Mason, 2013).

These changes will have implications for shallow water $CaCO_3$ mineral kinetics (Morse and Mackenzie, 1990), sediment shelf compositions, and potentially, marine ecosystems dependent upon skeletal and shell structures comprised of $CaCO_3$ minerals (Kleypas et al., 1999; Riebesell et al., 2000). The net loss of $CaCO_3$ materials may induce changes in coastlines that are directly created by $CaCO_3$ (i.e., calcareous sand beaches), or those that are shielded from hydrodynamic disturbance due to the baffling effect of offshore $CaCO_3$ ecosystems like coral reefs (Lowe et al., 2009; Andersson and Gledhill, 2013; Comeau et al., 2016). Ecosystems for which the formation of $CaCO_3$ substrates serve an important function, such as shallow water coral reefs, are of concern under continued OA as they provide a vital habitat for numerous other organisms and provide economic, cultural, and social benefits (e.g., Lugo-Fernández et al., 1998; Gratwicke and Speight, 2005).

Tropical surface ocean waters in the Caribbean show that calcification rates may have dropped by ~15 % with respect to their pre-industrial values (Friedrich et al., 2012), and Ω_{arag} is currently decreasing at a rate of about 3 % per decade (Gledhill et al., 2008; Bates et al., 2012). Perry et al. (2018) found that many shallow coral reefs across the Caribbean are very close to carbonate production and accretion thresholds due to the decline in live coral cover and sea level rise. However, the accretion rates and thresholds presented in Perry et al. (2018) may be lower since reef physical erosion and chemical dissolution were not included in the projections. Tropical near-shore coral reefs could have transitioned from net precipitation to net dissolution (e.g., Muehllehner et al., 2016), but attributing changes in net ecosystem metabolic rates to variations in carbonate chemistry remains challenging in coral reef ecosystems due to the multiple biogeochemical processes affecting coastal waters (Duarte et al., 2013).

Forecasting the effects of continued OA on coral reefs has relied heavily on laboratory and small-scale mesocosm manipulative experiments. The results of these experimental manipulations are often applied to projections of surface ocean carbonate chemistry derived from coupled climate/carbon-cycle models (e.g., Cao and Calderia, 2008). However, most coastal systems exhibit considerably greater complexity than those reproducible in laboratories and expressed in these global models. Seasonal and diurnal variations in seawater carbonate chemistry and Ω_{arag} within the reef zone can be several times higher or lower than expected for oceanic waters due to net ecosystem metabolic processes alone (Gattuso et al., 1993; Bates et al., 2010; Turk et al., 2015; Page et al., 2017). The net ecosystem production (NEP, the sum of gross production and respiration processes from all the autotrophic and heterotrophic components of the system) alters the dissolved inorganic carbon (DIC) and the $[H^+]$ concentration and thus can alter the relative partitioning of the carbonate species (Eq.1) and Ω_{arag}. Net ecosystem calcification (NEC, the sum of calcium carbonate production and dissolution processes from all biotic and abiotic components of the system) alters the seawater total alkalinity (TA) and DIC in a ratio of 1:2. The combination of NEP and NEC (under constant temperature, salinity, and pressure), change the seawater DIC:TA ratio, which dictates properties such as pH, CO_2 partial pressure ($pCO_{2,sw}$), and Ω (Zeebe and Wolf-Gladrow, 2001).

NEC and NEP measurements describe the net accumulation or consumption of inorganic and organic carbon, respectively (e.g., Gattuso et al., 1998). NEC can also be described in terms of the $CaCO_3$ gain and loss due to calcification and chemical dissolution processes. This is necessary to consider in order to quantify the total net accretion rates of the reef substrate (e.g., Eyre et al., 2014). Any decline in NEC relative to NEP could compromise many reef systems, since rates of accretion on healthy, undisturbed reefs only slightly outpace rates of reef loss due to physical and biological erosion (see Glynn and Manzello, 2015). Gradual changes in NEP and NEC can bring the system closer to a 'tipping point' where even small perturbations can cause a shift on the autotrophic-calcifying balance that characterized coral reef ecosystems, to a system dominated by heterotrophic and dissolving conditions (Silbiger et al., 2014; Yeakel et al., 2015). However, discerning whether these net ecosystem metabolic processes are changing due to natural ecological variability (e.g., changes in benthic communities) or because of anthropogenic

activities (e.g., eutrophication, OA) is non-trivial and demands sustained robust monitoring at a high temporal resolution, requiring *in situ* autonomous measurements and *in situ* water sampling.

Despite the importance of monitoring NEC and NEP using standard best-practices for sustained monitoring of these rates remains a major challenge. NEC and NEP measurements typically adopt various Lagrangian or Eulerian techniques requiring high-temporal resolution of *in situ* bottle water samples (e.g., Gattuso et al., 1996; Bates, 2002; Silverman et al., 2007). Recently, a few *in situ* autonomous methods have been proposed which offer great promise, but currently remain cost prohibitive for most networks, and have a limited duration of a few weeks at most due to biofouling and sensor drift (e.g., Yates et al., 1999; McGillis et al., 2011; Falter et al., 2008; Takeshita et al., 2016). Nevertheless, techniques and methods that incorporate existing observations of carbonate chemistry presently allow the development of net ecosystem metabolic proxies that could be employed to monitor these biogeochemical fluxes.

The time series presented here benefits from nine years (from 2009 to 2017) of continuous observations of the carbonate chemistry at the forereef of Enrique coral reef in Puerto Rico. The combined measurements obtained from the moored autonomous pCO_2 (MapCO_2) buoy technology with a dedicated discrete sampling campaign have provided high-quality observations allowing reasonable constraint of the carbonate system and of the biological processes affecting the water mass as it flows in over the reef platform from the open ocean end member. Moreover, the time series enables us to derive multi-year estimates of NEP and NEC using site-specific empirical relationships derived from both *in situ* autonomous and discrete bottle data.

In this manuscript, we described the seasonal variability and primary controls of the carbonate system variability and how such dynamics may change as a consequence of OA in the La Parguera near-shore reef system. In order to accomplish this, we tailored our approach to de-couple the biological processes on NEP and NEC, and derived seasonal net ecosystem metabolic rates for the reef system mixed layer using a one-dimensional (1-D) mass balance model developed with the autonomous MapCO_2 buoy observations. These metabolic observations serve to provide a more comprehensive interpretation of how

near-shore carbonate chemistry is governed by carbon cycling and to enhance our understanding of the potential long-term impacts of OA on carbonate and energy budgets.

2 Methods

2.1 La Parguera OA Time Series

The La Parguera OA time series (Fig.1) is an on-going project advanced by the NOAA Coral Reef Conservation Program (CRCP) that was established in 2009. The test-bed has since been adopted as a long-term sustained monitoring station providing physical, chemical, and ecological data under the National Coral Reef Monitoring Program (NCRMP, www.coris.noaa.gov/monitoring/) jointly sponsored by NOAA CRCP and the NOAA Ocean Acidification Program (OAP). Details about the efforts supporting this time series station are described in the supplemental material, S1.

2.2 Study sites

The Marine Reserve of La Parguera is located on the southwest coast of Puerto Rico (Fig.2-a). The well-developed reef system consists of different habitat types dominated by seagrasses, macroalgal beds, unconsolidated carbonate sediments, and mangroves. The reserve exists in an area with relatively low coastal development, an absence of local rivers, and the lowest rainfall rate in Puerto Rico (Pittman et al., 2010). Local environmental stressors include coastal runoff and fishing (Garcia-Sais et al., 2008).

The insular shelf extends 10-11 km from the coast and is divided in three different regions (inner, middle, and outer shelf reefs) according to its general morphological and depositional characteristics (details in Morelock et al., 1977). The MapCO_2 buoy is located at the west-end of the Enrique middle-shelf reef at 2.5 km from the coast and over the forereef where the water depth is about 3 m (Fig.2-c).

Cayo Enrique is an emergent reef adjacent to a mangrove system. The back reef and reef flat areas consist of seagrass beds dominated by *Thalassia testudinum* and a few coral patch reefs. The forereef and the upper zone benthic reef communities at Enrique were formerly dominated by the branching coral *Acropora palmata*. Significant live coral cover was reduced by >50 % from 2003 to 2007 (Appeldoorn,

2009). Losses in coral cover are attributed to coral bleaching and disease, and secondarily from hurricanes, and corallivorous mollusks (Morelock et al., 2001; Ballantine et al., 2008). The die-off of the long-spined sea urchin, *Diadema antillarum* limited coral recovery and prevented recruitment to bare substrates due to the increased algae cover (Ballantine et al., 2008). Currently, most of the area formerly covered by *A. palmata* is dead and replaced by *Millepora* spp., *Palythoa caribaeorum* (zoanthids), and soft corals such as *Gorgonia* spp. and *Pseudopterogorgia* spp. McGillis et al. (2011) and Manzello et al. (2017) noted approximately 10 and 11 % live coral cover area during belt transect surveys at the MapCO_2 area in March 2009 and August 2015, respectively. The six major reef building corals reported by McGillis et al. (2011) were: *Siderastrea siderea*, *Porites astreoides*, *Pseudodiploria strigosa*, *Siderastrea radians*, *Pseudodiploria clivosa*, and *Porites porites* (ranked in order of areal cover). The dominant benthic communities reported by Manzello et al. (2017) were: sand (30%), soft coral (25%), turf algae (17%), sponges (10%), and coral rubble (5%). A survey conducted in 2011 by Moyer et al. (2012), showed that the non-calcifying algal cover was ~ 25 %, with little seasonal variation. However, Pittman et al. (2010) reported a peak of turf algae and macroalgal cover in the summer. Calcifying algae (crustose coralline algae) represent about 1 % of the benthic cover with no significant seasonal variation (Pittman et al., 2010; Moyer et al., 2012).

The sediments at the forereef of Enrique consist predominantly of $CaCO_3$, with lesser amounts of terrigenous (<10 %) and organic material (Ryan et al., 2008; Hernández et al., 2009). According to Morelock et al. (1977) the major $CaCO_3$ contributors are fragments of calcareous green algae (*Halimeda* spp.), coral fragments (40 to 80 %), and coralline-algae (10 to 20 %). It is possible that the relative proportions of the sediment composition and re-distribution have changed over the last 40 years during high-wave energy events (e.g., hurricanes and storms). However, Hernández et al. (2009) found that $CaCO_3$ minerals are still the predominant sediment type at the site, dominated by aragonite and Mg-calcite with 13-14 mol % $MgCO_3$, and with lesser amounts of ~3 mol % $MgCO_3$. These are produced *in situ* by bioerosion and mechanical processes (Hernández et al., 2009).

NEP rates were estimated at Enrique forereef during March of 2009 using the boundary layer O_2 gradient and enclosure methods (McGillis et al., 2009; McGillis et al., 2011). The average daily NEP rate were 43.1 and 60.3 mmol C m^{-2} d^{-1} (converted from O_2 to C using the Redfield molar ratio of 138:106) for both methods respectively (McGillis et al., 2011). Results from both methods suggested that during the time of these experiments organic carbon respiration contributed CO_2 to reef waters. During the same study the ocean current speeds were measured using a set of ADCPs. The average current speed ranged between 2 to 10 cm s^{-1} towards the west.

Reef areas are flushed by offshore water and typically have water residence times of days to weeks, while longer residence times (months) are found closer to shore (Venti et al., 2012). The residence times from the offshore station and Enrique reef (Fig.2) were measured in 2011 using the inputs and outputs of Beryllium-7 (^{7}Be) according to Venti et al. (2012, 2014). The mean residence times calculated for January and May were 9 and 11 ± 2 days (Venti, personal communication), respectively.

2.3 Autonomous observing capabilities and dataset

The autonomous capability of the Ma*p*CO_2 buoy provides continuous 3-hour measurements of both $CO_{2,air}$ and $CO_{2,sw}$ mole fraction ($xCO_{2,air}$ and $xCO_{2,sw}$). These are converted to *p*CO_2 with total uncertainties of <1 µatm and <2 µatm, respectively (Table 1; Sutton et al., 2014a). The buoy is equipped with a seawater-gas equilibrator, reference gas standard, an infrared gas analyzer, Seabird 16/37 conductivity and temperature recorder, and a Sunburst™ SAMI-pH system located at about 1 m depth. Details of the Ma*p*CO_2 instrument calibration and data Quality Assurance and Quality Control (QA/QC) processes are described in Sutton et al. (2014a, 2014b). Final measurements used for the analyses cover from January 2009 to January 2017.

The Ma*p*CO_2 buoys also have an internal Maxtec™ O_2 sensor (MAX-250+) located inside the CO_2 electronics tube (downstream of the infrared gas analyzer sensor) to measure percent of oxygen in air (% O_2, ± 3%). These sensors are part of the observational network of all PMEL CO_2 buoys, but only intended as a diagnostic tool. The sealed compartment that houses the sensor provides protection from seawater

and the effects of marine biofouling, and excessive temperature, humidity, and pressure changes. Despite their diagnostic purpose, they have been shown to offer some utility for studying ocean biological variability (e.g., Xue et al., 2016) even though measurements from the MAX-250+ may not be ideal due to slow O_2 equilibration response times (Sutton et al., 2014a). Nevertheless, in an effort to achieve more coherent and usable long-term estimates of O_2 concentrations, we obtain reasonable results when we post-calibrate the MAX-250+ using early deployment data from the Aanderraa™ O_2 optode (Aanderaa 4775, accuracy of ±5 %).

The O_2 data obtained by the optode sensor tends to be unreliable for extended deployments of over 6 months as a consequence of biofouling and subsequent sensor drift. Therefore, we proceed under the assumption that they are accurate within specifications for a time period between calibration and prior to any biofouling. The MAX-250+ sensor bias correction was derived from four optode deployments from 2011 to January 2017, and 20 *in situ* bottle Winkler O_2 (Winkler, 1888) measurements collected and analyzed at the CARICOOS lab between 2015 and 2016. The O_2 optode measurements were salinity compensated and an internal QA/QC process was applied where the first O_2 measurements were removed (considered as the flush to purge residual water and bubbles in the flow lines) and the last two of each cycle averaged. Seawater surface concentration (mmol m^{-3}) is calculated using the O_2 solubility (Garcia and Gordon, 1992) as a function of SST and SSS. Linear regression analyses were performed at daily and seasonal time scales (see supplemental material, Fig.S1 and S2) and the best fit (r^2 = 0.90, RMSE = 3, n = 40) was found using the daily averages of the first 40 days after the first deployments, a time interval whereby we judge the data accurate. We corrected the MAX-250+ measurements using the offset and slope (Fig.S1). We also found the corrected O_2 measurements agreed reasonably well with the Winkler O_2 determinations (± 6.85 mmol m^{-3}).

Hourly wind measurements were taken from the nearby NOAA Integrated Coral Observing Network (ICON) station. This station was maintained as an instrumented Coral Reef Early Warning System (CREWS) station from 2006 to 2013 at the Media Luna middle-shelf reef (Fig.2-b), located 1.8 km south from the MapCO_2 buoy. In 2015, CARICOOS established a meteorological station at the nearby Marine

304 Lab (Fig.2-b), 1.5 km from the MapCO_2 buoy. Wind speed from the ICON and CARICOOS stations were
305 measured at 6.5 m and 7.8 m height, respectively. Wind speeds were normalized to a wind speed at 10 m
306 height according to Hsu et al. (1994) and averaged to every 3 hours. Wind data is taken from this station
307 from 2015 to 2017. Wind data gaps were filled using a climatological curve created with these two
308 datasets. This method was preferred over the use of buoys far from the near-shore study site or satellite
309 wind measurements, as their use tends to overestimate the gas air-sea exchange due their low temporal
310 coverage and limited near-shore spatial coverage (e.g., Jiang et al., 2008). We believe that the coastal
311 topographic setting plays a role in setting up diurnal wind patterns, which are not captured by the remote
312 buoys or the satellite-derived wind speed data.

313 **2.4 *In situ* geochemical surveys**

314 Open ocean dynamics in carbonate chemistry are reasonably well constrained and often characterized
315 based on TA-salinity and pCO_2-temperature relationships (Lee et al., 2006; Gledhill et al., 2008).
316 However, in near-shore environments benthic and coastal processes can convolute these relationships.
317 Therefore, the autonomous observations were validated and supplemented on a weekly (2009-2013) and
318 bi-weekly (2013-2017) basis through direct measurements of potentiometric TA and spectrophotometric
319 pH. Phosphate and silicate concentrations were collected at the buoy site and measured according to
320 Strickland and Parson (1972) six times over the period from 2009 to 2011 in January, February, March,
321 May, November, and December. Details about the collection and analyses procedures of these *in situ*
322 measurements are available in supplemental material, S2.
323
324 The average difference between $pCO_{2,sw}$ buoy measurements and $pCO_{2,sw}$ calculated from *in situ* bottle
325 samples was <0.5 µatm. The average difference between SAMI-pH and spectrophotometric pH
326 measurements was 0.005. This data comparability, achieved with widely differing methods, demonstrates
327 the robust quality of our analytical procedures and resulting data. *In situ* bottle measurements helped with
328 the determination of site-specific algorithms for TA and allowed estimates of DIC and $pCO_{2,sw}$ from *in*
329 *situ* bottle samples (described in Sect. 2.6.4). These data sets were also used to investigate factors

Biogeosciences Discuss., https://doi.org/10.5194/bg-2018-408
Manuscript under review for journal Biogeosciences
Discussion started: 12 October 2018

330 controlling the $pCO_{2,sw}$ dynamics at the reef station using a 1-D mass conservation model (described in
331 Sect. 2.6).

332 **2.5 First-order derivations of TA and calculation of carbonic acid system**

333 TA algorithms based on seawater surface salinity (SSS) and temperature (SST) break down for inshore
334 waters subject to contributions from multiple freshwater end-members and CO_3^{2-} ion variability during
335 calcification and dilution processes (Lee et al., 2006), requiring site-specific relationships to be
336 determined. At the Enrique forereef, *in situ* bottle TA measurements showed a moderate ($r^2 = 0.42$), but
337 robust ($p < 0.0001$, $n = 547$) correlation to SSS (see supplemental Fig.S3). This was improved with the
338 weak ($r^2 = 0.27$), but significant ($p < 0.0001$, $n = 548$) negative correlation with SST. The resultant
339 multivariate linear relationship between TA with SSS and SST produced an $r^2 = 0.55$ and $p<0.001$ (n=
340 547, RMSE = 30). This was used to model TA ±30 µmol kg^{-1} at the reef (TA_{reef}):
341
342 $$TA_{reef} = 43.2(\pm 0.08) \times SSS - 12.5\ (\pm 0.07) \times SST + 1118\ (\pm 2.10) \quad (5)$$

343 where, the ± is the standard error of the coefficients.
344
345 The reef CO_2 – carbonic system was fully solved using TA_{reef} and the $pCO_{2,sw}$, along with SSS, SST, and
346 pressure (1 db – pressure at 1 meter) from the buoy measurements. The MATLAB program CO_2SYS (van
347 Heuven et al., 2011), applying the dissociation constants for K_1 and K_2 of Lueker et al. (2000) and for
348 K_{HSO4-} from Dickson (1990), was used.

349 **2.6 Diagnostic mass budget model**

350 A 1-D mass budget model was used to calculate the net change in $pCO_{2,sw}$ based on contributions from
351 the processes controlling the variability of $pCO_{2,sw}$ at the surface (e.g., Gruber et al., 1998; Shadwick et
352 al., 2011; Fassbender et al., 2016; Xue et al., 2016). The model is assumed to provide an integrated
353 assessment of biogeochemical variability throughout the well mixed water column as the water mass
354 flows in over the reef-shelf platform from the open ocean end member. The net changes in observed
355 $pCO_{2,sw}$ (δpCO_{2OBS}) were calculated from mass the balance as given by:

Biogeosciences Discuss., https://doi.org/10.5194/bg-2018-408
Manuscript under review for journal Biogeosciences
Discussion started: 12 October 2018

$$\frac{\delta pCO_{2OBS}}{dt} = \frac{\partial pCO_{2\,SOL}}{\partial t} + \frac{\partial pCO_{2\,AIR-SEA\,EX}}{\partial t} + \frac{\partial pCO_{2\,HOR\,MIX}}{\partial t} + \frac{\partial pCO_{2\,BIO}}{\partial t} \quad (6)$$

where, the corresponding daily δpCO_{2OBS} are from the partial changes (∂) of gas solubility as a function of SST and SSS (SOL), air-sea exchange (AIR-SEA EX), horizontal mixing processes (HOR MIX), and biological activity (BIO). All the individual parameters used the observed daily means to avoid the effects of high frequency (<24 hr) processes (e.g., tides and diurnal biological activity). The data were binned within representative Julian days to create a composite year for each day from 2009 to 2017 (details in Sect. 2.9).

2.6.1 Thermodynamic variability

The thermodynamic variability (∂pCO_{2SOL}) was imposed on the system using daily-observed changes in SST and SSS using the CO_2SYS program. We preferred this method over the temperature only dependence coefficient ($0.0423°C^{-1}$) by Takahashi et al. (1993) as both SSS and SST impart thermodynamic variability in this region and the SST distributions are much different with respect to the waters on which this dependence was derived.

2.6.2 Variation by physical transport

The physical transport attributable to horizontal transport via advection ($\partial pCO_{2HOR\,MIX}$) was characterized empirically using SSS changes with assumed conservative mixing of TA and DIC between the reef and open ocean (e.g., Xue et al., 2016). Changes due to vertical mixing are neglected and the mixed layer is assumed to extend to the bottom given the small variations on SSS and SST, from the CTD casts performed for the *in situ* geochemical surveys, and shallowness of the site (3 m). In addition, three tidbit temperature loggers were deployed one year long from January through December 2015 at different depths along the buoy assembly, showing no thermal stratification in the area. The seasonal change in SSS due to the mean potential evapotranspiration to precipitation rate is assumed to be small (<0.1%) and hence neglected. Mixing due to tides is ignored due to the limited diurnal tidal range (<0.25m) in the area.

382 *In situ* bottle TA and DIC samples were obtained from seasonal cruises around the Caribbean Region
383 (details in supplemental material, S3), including three cruises to the Caribbean Time Series station (CaTS,
384 Fig.2-b). The linear relationship between TA and SSS measurements (n= 237, r2 = 0.99, p<0.001, RMSE
385 = 4.79) was derived to model TA (TA_{ocean}). To model DIC (DIC_{ocean}) a linear relationship (n= 220, r^2 =
386 0.93, p <0.001, RMSE = 12) with SSS and SST was derived. We used the observed daily change in SSS
387 at the buoy to estimate daily changes of TA and DIC from the conservative mixing relationships as
388 follows:
389
390 $$TA_{ocean}\ (\pm 4.79) = 58.9\ (\pm 0.02) \times SSS + (S_2 - S_1) + 237\ (\pm 0.900) \quad (7)$$
391 $$DIC_{ocean}\ (\pm 12) = 50.1\ (\pm 0.25) \times SSS + (S_2 - S_1) - 4.13\ (\pm 0.16) \times SST + 322\ (\pm 12.5) \quad (8)$$
392
393 where, the ± is the standard error of the coefficients or the RMSE of the derived quantity as applicable,
394 and S_1 and S_2 correspond to the salinity at time 1 and 2, respectively. Despite the large uncertainties
395 reported for the physical term using the mass conservation model approach (e.g. Shadwick et al., 2011;
396 Fassbender et al., 2016; Xue et al., 2016), the effect of such uncertainty on subsequent derivations is
397 minimal (details in Sect. 2.10).

398 **2.6.3 Air-Sea exchange**

399 The effects on $pCO_{2,sw}$ due to the physical transport through the air-sea CO_2 exchange ($\partial pCO_{2AIR\text{-}SEA\ EX}$)
400 is related to the DIC changes and air-sea CO_2 flux (F_{CO2}). The $DIC_{AIR\text{-}SEA\ EX}$ (µmol kg^{-1} day^{-1}) is estimated
401 via the change in mixed layer DIC inventory as:
402
403 $$DIC_{AIR-SEA\ EX} = \frac{ks \times (fCO_{2,sw} - fCO_{2,air})}{h\rho} \quad (9)$$
404
405 where, $fCO_{2,sw}$ - $fCO_{2,air}$ is the difference in atmospheric and seawater CO_2 fugacity (fCO_2) concentration,
406 calculated from the $xCO_{2,air}$ and $xCO_{2,sw}$ buoy measurements and converted according to best practices
407 (Dickson et al., 2007; SOP 5) using the virial coefficient of pure CO_2 and the virial coefficient of $CO_{2,air}$

408 according to Weiss (1974). The s (mol kg^{-1} atm^{-1}) is the solubility of CO_2 per unit volume of seawater
409 (Weiss, 1974), k (m s^{-1}) is the transfer velocity as a function of wind speed at 10 m above mean sea level,
410 h is the mixed layer water depth (m), and ρ the seawater density (kg m^{-3}). The transfer velocity-wind
411 speed relationship used is described by Wanninkhof (2014). As a convention in this paper, O_2 and CO_2
412 positive fluxes are from the ocean to the atmosphere.

413 **2.6.4 Modulation carbonate parameters by biological processes**

414 The biological processes affecting $pCO_{2,sw}$ (∂pCO_{2BIO}) were estimated as the residual of the remainder of
415 the other terms on the mass conservation equation (Eq.6) to close the system. The changes on ∂pCO_{2BIO}
416 due to biological activity were defined as:
417

418 $$\frac{\partial pCO_{2\,BIO}}{\partial t} = \frac{\partial pCO_{2\,NEP}}{\partial t} + \frac{\partial pCO_{2\,NEC}}{\partial t} \quad (10)$$

419

420 where pCO_{2NEP} is defined as the processes affecting $pCO_{2,sw}$ due to gross photosynthetic production and
421 community respiration and the pCO_{2NEC} refers to the processes affecting $pCO_{2,sw}$ due to calcium carbonate
422 gross calcification and gross dissolution.
423

424 The Revelle Factor (β, $\partial \ln pCO_{2,sw}$ /$\partial \ln$ DIC) was used to convert changes in ∂pCO_{2BIO} to changes in DIC
425 (∂DIC_{BIO}) using the relation between $pCO_{2,sw}$ and DIC as defined by Revelle and Suess (1957). The *in*
426 *situ* bottle pH and TA measurements were used to calculate the *in situ* bottle $pCO_{2,sw}$, the DIC, and the β.
427 The partial change in DIC due to $pCO_{2,sw}$ (DIC/$pCO_{2,sw}$,, μmol kg^{-1} μatm^{-1}) was related to β. This was
428 linearly related to changes in SST (n = 467, r^2 = 0.86, p <0.001, RMSE = 1.02; Fig.3). The ∂pCO_{2BIO} was
429 converted to ∂DIC_{BIO} according to the following relationship:
430

431 $$\frac{\partial DIC_{BIO}}{\partial t} = \frac{\left(\frac{DIC}{pCO_2} \times \frac{\partial pCO_{2BIO}}{\partial t}\right)}{\beta} \quad (11)$$

432

Biogeosciences Discuss., https://doi.org/10.5194/bg-2018-408
Manuscript under review for journal Biogeosciences
Discussion started: 12 October 2018

2.7 Net Ecosystem Production (NEP) and Net Ecosystem Calcification (NEC) rates

The difference between gross ecosystem photosynthetic production and respiration (NEP) was addressed using the observed O_2 (O_{2OBS}) measurements and the net O_2 air-sea flux (F_{O2}). The net change in O_2 due to organic production is defined as:

$$\frac{\partial O_{2NEP}}{\partial t} = \frac{\partial O_{2OBS}}{\partial t} - \frac{\partial O_{2GAS}}{\partial t} \quad (12)$$

where, ∂O_{2OBS} (mmol m^{-3}) are the O_{2OBS} changes and the ∂O_{2GAS} (mmol m^{-2} day^{-1}) are the O_2 changes due to F_{O2}. The O_2 fluxes were calculated using the transfer velocity (details in Sect. 2.6.3) and corrected by the bubble flux injection and the bubble flux exchange (Manning and Nicholson, 2016). The changes on O_{2NEP} were converted to those of carbon using the Redfield carbon to oxygen molar ratio of 106:138 (close to the observed O_2 to DIC ratio of 1.1 at Enrique reef) and integrated over the mixed layer.

The NEC was estimated using equations (11) and (12) as follows:

$$\frac{\partial DIC_{NEC}}{\partial t} = \frac{\partial DIC_{BIO}}{\partial t} - \frac{\partial O_{2NEP}}{\partial t} \quad (13)$$

2.8 Ecosystem free energy budget

We recast our monthly Ω_{arag} climatology in terms of free energy by applying equation 4 and the equations detailed in Morse and Arvidson (2002) for three common mineral phases relevant to coral reef ecosystems: aragonite, 10% $MgCO_3$, and 15% $MgCO_3$. From the monthly climatological Ω_{arag} values generated from CO_2SYS we first derived the ion concentration product (*ICP*) using the stoichiometric solubility product (K^*_{SP}, Eq.3) and subsequently converted it to *IAP* using the ratio of the thermodynamic to stoichiometric solubility products according to:

$$IAP = k_x \Omega_x \quad (14)$$

459

460 where, k_x is the thermodynamic solubility product for x calcium carbonate mineral phase (Plummer et al.,
461 1978).

462 **2.9 Constructing an annual climatology**

463 We use the average daily observations from 2009 to 2017 to construct the annual climatology for each
464 parameter and derived products to examine the seasonal cycles. The composite year was constructed by
465 binning the data within the representative Julian day. The time series was compiled into two distinct
466 seasons based on the weather in Puerto Rico. The dry and cool season extends from October to March,
467 considered winter. The rainy, humid and hot period runs from April to September and is defined as
468 summer. The seasonal variability was computed using the peak-to-peak amplitude. Details about how the
469 gaps were filled are described in the supplemental material, S4.

470 **2.10 Error assessments**

471 Model errors for the mass budget model variables (Eq. 6), NEP, and NEC were estimated using Monte
472 Carlo simulations. The same approach was used to estimate the uncertainties of TA_{reef}, DIC_{reef}, $DIC_{AIR\text{-}SEA\ EX}$,
473 DIC_{BIO}, Ω_{arag}, and β linear regression coefficients. Prior to the Monte Carlo simulations, a
474 normality check was performed using the Kolmogorov-Smirnov test on each of the model variables to
475 verify that the data were normally distributed. Random normal distributions of each model variables
476 (Table 1) were generated using MATLAB. Sampling was repeated 1,000 times to establish the final
477 uncertainty, mean, and standard deviation for each simulation. Details about the error analyses are
478 describe in the supplemental material, S5.

479

480 The uncertainties associated with the buoy observations are relatively small compared with the
481 uncertainties in TA derived from the conservative mixing with SSS and SST (Eq. 5). This error is large
482 relative to the daily TA changes (which were typically small) and arises largely from non-conservative
483 biological processes, involved with net calcification and net dissolution, which cannot be captured in our
484 linear model. However, we demonstrate that TA uncertainties from the conservative mixing model are

less than the combined uncertainties on the TA anomaly technique from the seawater residence time and depth (Venti et al., 2012; Falter et al., 2013; Teneva et al., 2013; Courtney et al., 2016). The 1-D mass balance approach avoids the errors of the TA-anomaly method and provides accurate estimates of the physical and biological processes. However, better constraint of the TA_{reef} would certainly help reduce uncertainties in NEC.

2.11 Biogeochemical footprint

To better constrain the uncertainty in the horizontal advection term, we used underway measurements of SSS, SST, O_2, $pCO_{2,sw}$ collected in November 2016 and March 2017 that were intended to assess the spatial variability around the MapCO_2 buoy. These surveys extended from the buoy site to >1km offshore/inshore and incorporated averaged column velocity profiles at the buoy site. The maximum $pCO_{2,sw}$ change observed during these surveys was $< \pm 0.5$ µatm day $^{-1}$ assuming the maximum observed current speed (7 cm s^{-1}) recorded. Our estimated uncertainty of pCO_2 ($\pm$ 0.5 µatm day $^{-1}$) is based on this observation. Considering a unidirectional ~7 cm sec^{-1} current, a daily mean parameter could be influenced by waters up to ~6 km from the buoy. In actuality, the length scale would be much less considering diurnal changes in tides and wind direction. Further, gradients in carbonate parameters between the different reef sites, seagrass, mangrove channels, sand, and offshore waters tend to be small relative to the temporal changes addressed in this study. Based on these results and Enrique's physicochemical characteristics (e.g., currents, winds, residence times, and SSS changes), we assume that the local river inputs are small and that the forcing from offshore waters occurs at time scales much longer than the reef residence time. Nevertheless, it is important to note that our estimates are not solely influenced by a single reef community and instead are representative of the broader reef-shelf complex system.

Biogeosciences Discuss., https://doi.org/10.5194/bg-2018-408
Manuscript under review for journal Biogeosciences
Discussion started: 12 October 2018

3 Results

3.1 Seasonal variability of the carbonate chemistry

On an annual scale, the Enrique reef experiences a seasonal SST daily average variations of about 4 ˚C (Table 2) with a maximum 30.2˚C during the summer (September) and a minimum of 26.6˚C during the winter (January). The SST at the reef is about 1 ˚C warmer and 1 salinity unit fresher than the offshore station CaTS. The high temperatures (>30 ˚C) between August and October coincide with low salinities (Fig.4-a). The SSS seasonal change is about 2 units with a maximum during the summer (April) and a minimum during the winter (November). Increased local rainfall causes recurrent decrease in SSS during the months of June through December. The DIC_{reef} and TA_{reef} show similar SSS seasonal patterns with maxima in April and minima between September and November (Fig.4-b). The DIC shows a smaller seasonal amplitude (~70 µmol kg^{-1}) compared with TA (~100 µmol kg^{-1}). Average phosphate and silicate concentrations were 0.032 ± 0.018 µmol L^{-1} and 1.83 ± 0.277 µmol L^{-1}, respectively. The TA changes attributable to these inorganic nutrients at these concentrations are negligible.

Enrique forereef, like many other reefs, is a persistent source of CO_2 to the atmosphere (2.04 ± 2.13 mmol CO_2 m^{-2} day^{-1}) with a minimum during the winter and a maximum during the summer (Fig.4-c, Table 2). The seasonal amplitude of the F_{CO2} is about 7 mmol CO_2 m^{-2} day^{-1} with an annual mean of 0.75 ± 0.78 mol CO_2 m^{-2} $year^{-1}$. Conversely, the maximum net F_{O2} outgassing (14 mmol O_2 m^{-2} day^{-1}) from the ocean to the air occurs during the winter. During the summer, the system is a net sink with a maximum of about -90 mmol O_2 m^{-2} day^{-1} (Fig.4-c, Table 2). Average daily wind speed ranges from 3 m s^{-1} to 6 m s^{-1} and prevailing wind direction from the east and southeast, with little seasonal variation (Fig.4-f, Table 2). The injection of bubbles represents <2 % of the total O_2 flux variation at the site.

Figure 4-d shows the $pCO_{2,sw}$, $pCO_{2,air}$, and O_2 dynamics for the site. Maximum seawater $pCO_{2,sw}$ values were observed from August through October (late summer) while minima occurs in February when the surface $pCO_{2,sw}$ decreases to near atmospheric equilibrium (~390 µatm). The $pCO_{2,sw}$ seasonal amplitude is about 70 µatm (Table 2). In contrast, $pCO_{2,air}$ fluctuations were modest (13 µatm) and similar to regional

$CO_{2,air}$ values reported (Conway et al., 1994; Masarie and Tans, 1995). Maximum $CO_{2,air}$ concentrations are observed from January to May (late winter) and minimum from June through October (late summer). The O_2 minimum (154 µmol kg^{-1}) occurs during the late summer when the $pCO_{2,sw}$ is at a maximum. The annual range of O_2 concentration is about 38 µmol kg^{-1} with a maximum (192 µmol kg^{-1}) during the winter.

The pH and Ω_{arag} show similar patterns with minimum values from August to November (pH <8 and Ω_{arag} <3.5) and maximum from March to May (Table 2). The mean pH is 8.02 ± 0.01 with an annual amplitude of 0.07 units. Mean reef pH conditions during the late summer are ~17 % lower ("more acidic") when compared with the winter (Fig.4-e). The mean Ω_{arag} is 3.59 ± 0.07 with an annual amplitude of 0.3 units (Table 2). These results are comparable with the seasonal results on Sutton et al., (2016) using the same data set from December 2012 to December 2014.

Results from the 1-D mass balance model results shows that the increase in ∂pCO_{2SOL} from May to mid-October can increase water column $pCO_{2,sw}$ up to about 20 µatm (Fig.5). During the same season, the air-sea exchange drives the $pCO_{2,sw}$ up to about 2 µatm decreasing DIC in the water column by only ~5 µmol kg^{-1}. From July through December, the ∂pCO_{2BIO} drives up the water column $pCO_{2,sw}$ by about 8 µatm. The $\partial pCO_{2HOR\ MIX}$ does not show a significant seasonal change and we find its contribution to be negligible (<1 µatm) throughout the year.

4 Discussion

4.1 Net Ecosystem Processes

High TA to DIC slope (>0.5) from the *in situ* surveys is observed in Enrique forereef indicating the strong influence of net ecosystem metabolic processes over DIC and TA (Fig.6). High TA to DIC slopes have been used to qualitatively suggest that the system shows net calcification. However, despite Enrique's high TA to DIC slope (1.1) calculated in this study and compared with other reefs areas in the Atlantic and Pacific by Cyronak et al., (2018), the excess of nTA and nDIC relative to adjacent Caribbean oceanic

values indicate that dissolution and respiration are dominant processes. Figure 6 shows how nTA and nDIC values are greater than the nTA and nDIC oceanic mean conditions (TA and DIC excess) indicating net ecosystem heterotrophy and carbonate dissolution conditions. It also shows that photosynthesis and calcification slightly dominate at some point in time when the TA and DIC values are below the oceanic mean conditions (TA and DIC consumption). This suggests that the CO_2 production during respiration could play an important role on pH and Ω_{arag} dynamics at seasonal time scales.

4.2 Physical and Biological drivers of $pCO_{2,sw}$

The 1-D mass balance model shows that throughout the year, solubility and biological changes are the dominant processes on the water column $pCO_{2,sw}$ dynamics at Enrique forereef (Fig.5). The solubility effects are driven by the small SST seasonal variation (4˚C), primarily due to the smaller amplitude in regional air temperatures and therefore, net atmospheric heat flux. The increase in SST during the early summer is the main driver increasing water column $pCO_{2,sw}$ and F_{CO2} from July to October. The SSS seasonal change is associated with the regional SSS dynamics from the extension of Amazon and Orinoco river plumes into the northeastern Caribbean (Corredor and Morell, 2001). The cooling and lower DIC pool from the freshwater influx of the regional river plumes have the opposite effect driving the $pCO_{2,sw}$ down. Biological processes (NEC and NEP) exert the second most important control on the $pCO_{2,sw}$ and F_{CO2} dynamics at this site on an annual scale (details in the next sections). The physical processes, i.e. horizontal transport and the removal of CO_2 from the mixed layer via air-sea exchange, play a small role on $pCO_{2,sw}$.

4.3 Net ecosystem metabolism rates

On an annual basis, the NEP is about 69.5 ± 9 g C m^{-2} $year^{-1}$ and NEC is about -581.9 ± 80 g $CaCO_3$ m^{-2} $year^{-1}$) at La Parguera reef shelf system. Under present day conditions the MapCO_2 buoy shows that both, dissolution and heterotrophic conditions persists for about 76 % (278 days) of the year in La Parguera reef system. This is longer than the time interval of dissolution found in the Pacific (Yates and Halley, 2006) and the Western Atlantic (Muehllehner et al., 2016). Our seasonal net ecosystem metabolic measurements are integrated over a longer time scales and spatial extent making difficult to compare with

studies that are based on short-time reef community diurnal experiments. However, at the uncertainties reported by other methods (e.g., TA-anomaly) this study may not be particularly anomalous in terms of dissolution considering that most of these studies are focused on a specific community. One of the caveats of the method is that is based on ecosystem processes in a near-shore reef zone that includes TA and DIC fluxes that do not originate from the reef. This could mask the coral reef biological signature. Additional studies would be required to evaluate and constraining these processes.

Based on our results, respiration is the major process dominating organic carbon metabolism at the site. Daily rates of NEP reef ranged from -11 to 67 mmol C m^{-2} d^{-1} (Fig.7-a). Negative NEP (NEP < 0) values represent net productivity (autotrophy) while positive (NEP > 0) values represent net respiration (heterotrophy). Results on McGillis et al., 2009; McGillis et al., 2011 from the gradient flux (CROSS) and enclosure (SHARQ) methods estimated NEP from March 27th - 29th of 2009 at Enrique reef of about 43.1 C mmol m^{-2} day^{-1} and 60.3 C mmol m^{-2} day^{-1}, respectively. Our results show an average of 26.3 mmol C m^{-2} day^{-1}. These rates are similar, but slightly less than the results from CROSS and SHARQ. We believe the discrepancy between estimates is mainly because our model uses measurements taken at the near-surface and thus integrates values over the water column and at some horizontal length scale. In contrast, the CROSS and SHARQ systems measurements are restricted to the benthic boundary. However, all methods showed net heterotrophic conditions during the studied days.

The seasonal rates of NEC range from -58 to 12 mmol $CaCO_3$ m^{-2} d^{-1} (Fig.7-b). Positive NEC values represent net calcification (NEC > 0) while negative values represent net dissolution (NEC < 0). The average dissolution rate of -22.6 mmol m^{-2} day^{-1} (-2.26 g m^{-2} day^{-1}), is at the higher end of rates reported for a coral reef system. Experimental studies have demonstrated that NEC rates are controlled by community composition and environmental conditions (e.g., Langdon and Atkinson, 2005). The high dissolution rates at Enrique forereef may be a function of the area occupied by reef-building corals at the site (~10%). Large reductions in live coral cover have occurred across the Caribbean (Gardner et al., 2003). This has caused a shift of reef community structure as most reefs are no longer being dominated by scleractinian corals and this has led to a decrease in calcification rates (Perry et al., 2013). Since our

model tracks the temporal behavior of TA, our high net dissolution rates could be influenced by TA subsidies not accounted for in this study. This includes biotic and abiotic processes at the carbonate sediments and coral rubble that cover around 35% of the Enrique forereef benthic area. For example, net dissolution rates have been reported for soft bottom/sediment communities (Boucher et al., 1998) and sand (Yates and Halley, 2006) at a rate of -2.4 mmol m^{-2} d^{-1} and -3.2 mmol m^{-2} d^{-1}, respectively. Another source of TA may arise via anoxic processes in the benthic community (e.g., sulfate reduction).

We consider that the 1-D mass balance approach using buoy $pCO_{2,sw}$ and O_2 observations produces similar NEC and NEP values as the "slack water" (e.g., incubations or mesocosms) and non-enclosure approaches (e.g., gradient flux, Eularian, Lagrangian and control volume of the seawater overlying the benthic community). Our method also addresses their combined influence of benthic and water column processes as well as the effects of $CaCO_3$ dissolution on net ecosystem processes within the mid-shelf reef areas of La Parguera Marine Reserve. It must also be pointed out that our mass balance approach does not provide absolute values for NEP and NEC, but rather provides a climatological view of seasonal changes in the balance of net heterotrophy and net autotrophy and net calcification and net dissolution. We submit that this could prove more useful in terms of coral reef management as a tool to monitor the reef system health across different temporal scales.

Further studies to validate this method against other methods that can capture the seasonal variability on NEP and NEC at the site are needed. Validation of the NEC and NEP estimates from this method, either directly or from nutrient or oxygen inventories, along with an understanding of hydrodynamics are needed to constraint the effective footprint of the buoy measurements and to better discern community responses. These additional assessments are necessary to predict the rates and magnitude of OA in near-shore reef ecosystems.

4.4 Seasonal dynamics and physical drivers of net ecosystem metabolism

The seasonal cycle of NEP indicates that most of the net organic carbon fixation occurs during the winter (Fig.7-a). This resulted in pCO_2 values close to atmospheric equilibrium. At the beginning of the winter

641 season (December) the system begins to switch from being heterotrophic to autotrophic, indicating that
642 community photosynthetic production in the winter is larger than the respiration (from December to
643 March). While production is an important process throughout the winter, respiration, particularly from
644 June and October, generates a local source of DIC to the system.
645
646 Gray et al. (2012) observed the same seasonal over-saturation of $pCO_{2,sw}$ at nearby Media Luna reef
647 during the summer and fall months from 2007 to 2008 and suggested that net heterotrophy was driven by
648 remineralization of mangrove-derived organic carbon inputs. We speculate that the main drivers of the
649 carbon excesses from mid-April to mid-December include a combination of exposure to exogenous
650 organic carbon sources from inshore mangrove channels and local red mangroves stands. The shoreline
651 of La Parguera urban area is influenced by increased nutrients and turbidity from terrigenous sources
652 (Otero and Carbery, 2005), which would also contain dissolved and particulate organic matter. Such
653 fluxes have been reported as primary threats to near-shore coral reef ecosystems (Garcia-Sais et al., 2008).
654 Observed heterotrophy also coincides with the wet season and the seasonal decrease in SSS caused by the
655 remote influx of freshwater originating from the Orinoco and Amazon River plumes (Corredor and
656 Morell, 2001). Inputs of coastal dissolved organic matter (DOM) and particulate organic matter (POM)
657 from these remote sources may significantly contribute. Continued investigation on coastal organic matter
658 components from local and remote sources will provide additional information on the sources of this
659 excess carbon.
660
661 We show that net calcification in Enrique forereef is coincident with maximum autotrophy, corresponding
662 with high Ω_{arag} and pH. It appears that the increase on net productivity and SSS from January to March
663 may enhance Ω_{arag} providing favorable conditions for calcification. This is consistent with the coral reef
664 ecosystem feedback hypothesis (CREF, Bates et al., 2009), where increasing Ω_{arag} is stimulated by an
665 increase in net productivity. The combined seasonality in solubility (SST and SSS), and net ecosystem
666 metabolic processes at the site act synergistically to exacerbate OA by depressing surface Ω_{arag} and
667 calcification from April to December. Therefore, net ecosystem metabolic processes provide positive
668 feedback driving Ω_{arag} down (Fig.8). Namely, continued release of CO_2 due to respiration from April to

December keep Ω_{arag} and pH low, driving metabolic dissolution (Anderson and Gledhill, 2013) which in turn increases pCO_2 and lowering pH.

The seasonal correlation of Ω_{arag} and NEC with SST and SSS is shown in Figure 9. The transition of NEC from net calcifying to net dissolving occurs in April when the seawater Ω_{arag} is <3.6, SST is > 27, and SSS is < 35 (Fig. 9). The biological effects exhibit hysteresis in NEC and Ω_{arag}, while the horizontal range shows the thermodynamic effects on Ω_{arag}. This is a characteristic of dynamic systems when multiple drivers can exist for the same set of parameter values (e.g., NEC or NEP). These seasonal shifts can be due to the combined synergy of local terms (thermodynamics, nutrients, light availability and water flow) and regional (river inputs) processes that can influence reef metabolism (e.g., Yeakel et al., 2015; Bates, 2017). Enrique reef shows that when thermodynamic effects increase and Ω_{arag} is high (>seasonal mean) the system starts shifting to net calcification and autotrophic conditions (winter: January to March). As the SSS decreases, the SST increases, and Ω_{arag} decreases below the seasonal mean. During this time the conditions are net heterotrophic and net dissolution rates increase, relative to the values above the Ω_{arag} seasonal mean. The underlying NEC- Ω_{arag} seasonal hysteresis reflect that Ω_{arag} is not the main driver of NEC and that NEP and SST seems to control carbonate precipitation at this site.

4.4 Net dissolutional conditions

The average net dissolution at Enrique is about 4 times more than calcification. On an annual basis, the loss in carbonate mass observed in La Parguera from April to December is about 629 ± 1.6 g $CaCO_3$ m^{-2} $year^{-1}$, a significant (*t*-test, p <0.0001) fraction of the winter calcification rate (40 ± 0.28 g $CaCO_3$ m^{-2} $year^{-1}$). Considering only the entire forereef area of Enrique (0.0656 km^2; Zayas, 2011), this corresponds to a loss of 45 tons of $CaCO_3$ vs 2.9 tons of $CaCO_3$ precipitated. These results indicate that La Parguera shelf reef systems are losing $CaCO_3$ by the process of metabolic dissolution at a rate far faster than production and has already crossed a threshold point for net positive carbonate production.

Enrique reef is well below the boundary point for where it has been shown that Caribbean reefs shift from net accretion to net erosion (Perry et al., 2013, 2015). Critical calcification/dissolution threshold values have been estimated to occur when $pCO_{2,sw}$ between the 450 - 1000 µatm and Ω_{arag} <3 (Langdon et al., 2003, Yates and Halley, 2006; Silverman et al., 2007; Andersson et al. 2009; Shamberger et al., 2011; Turk et al., 2015). These thresholds vary from one reef to another as a consequence of benthic community composition, structural complexity (i.e., reactive surface area), variations in residence times (which effect the time-space integration), light, hydrodynamics, and nutrient availability (Yates and Halley, 2006; Silverman et al., 2007; Shamberger et al., 2011). Such thresholds are also dependent on the % of live coral cover and the combination of erosional, dissolution, and bio-erosional processes at the reef (Perry et al., 2013).

Our model estimates show the system exhibiting net $CaCO_3$ dissolution (NEC <0) on an annual basis, although Ω_{arag} does not exceed the Ω_{arag} and $pCO_{2,sw}$ thresholds suggested by others. Indeed, dissolution rates at Enrique reef are higher than the levels projected for the 21st century (Eyre et al., 2018). Although, most modern tropical coral reef systems currently reside well above potential critical thresholds to maintain net reef calcification or accretion (Guinotte et al., 2003; Perry et al., 2013, 2015), near-shore Caribbean coral reefs with low live coral cover could have reached these tipping points due to disease and bleaching (linked to high SST), leading to low rates of NEC. For example, discrepancies are found with the results from the census-based carbonate budget data collected at Enrique reef in August 2015 reported a mean net $CaCO_3$ production 1.04 (± 1.26) kg m^{-2} $year^{-1}$ and an accretion rate of 0.55 ± 0.62 mm $year^{-1}$ (Perry et al., 2018). This method suggests that the Enrique reef exhibited positive accretion, albeit minimally and with high variability. These budget surveys are not directly comparable to our NEC rates, as they do not incorporate chemical dissolution and they are based on data obtained from a single point observation in time. In addition, the census approach is based on the sum of the literature estimated calcification rates by individual $CaCO_3$ producers whereas our approach integrated abiotic and biotic processes over the entire reef system. Our current estimates are controlled by a combination of the open ocean end member and biogeochemical and hydrodynamic processes on the reef shelf. The results from these studies highlight the need to develop methods to better understand the metabolic processes and

723 seawater chemistry across functional, spatial, and temporal scales. Further refinement of our model is
724 required to better understand the carbonate chemistry variability at each functional community scale.
725
726 The highest rates of net dissolution occur during periods when rates of net heterotrophy are at their
727 highest. This corresponds to the periods when highly soluble minerals, cements, and organisms such as
728 crustose coralline algae exhibit net dissolution. An increase in the magnitude or time of occurrence of net
729 dissolution could become a serious threat to the formation of sediments, reefs, and other structures
730 composed of $CaCO_3$ (Eyre et al., 2014; 2018). It is clear, that under continued periods of net dissolution,
731 net reef accretion is jeopardized in the face of other climate stressors (e.g. coral bleaching and ocean
732 warming). Our model, coupled to the MapCO_2 data provides the ability to monitor and understand near-
733 shore carbonate chemistry variability to assess, forecast, and model the impacts of OA on near-shore reef
734 ecosystems. Prior to design of measures that may effectively ameliorate the impact of OA on tropical
735 shallow coral reefs ecosystems and allow us to improve current management strategies; we need to
736 develop a detailed understanding of the carbon cycle role in net ecosystem metabolic "performance". This
737 will aid in the identification and development of effective adaptation mitigation strategies that could
738 reduce local carbon inputs and decrease erosional processes.

739 **4.5 Free energy dynamics at La Parguera Near-Shore Reef ecosystems**

740 The use of Ω_{arag} as an index of coral health has perhaps been over-utilized in the OA literature to date,
741 with few instances of explicit acknowledgment of what the index truly represents nor the key assumptions
742 implied when adopting its use. Firstly, when considering the use of Ω_{arag} within the context of a coral reef
743 ecosystem, it should be appreciated that a coral reef comprises a heterogeneous composition of a range
744 of $CaCO_3$ minerals. While aragonite dominates, considerable amounts of magnesium carbonate with
745 variable ranges in magnesium content are also present. Furthermore, the stoichiometric solubility product
746 used by CO2SYS to generate the Ω_{arag} value is experimentally derived using abiotic aragonite while the
747 vast majority of $CaCO_3$ minerals deposited on coral reefs are biogenically derived. The behaviour of these
748 biogenically produced minerals is complex in seawater owing to the important role of kinetics so care
749 must be taken to avoid over-interpreting a reported saturation state with a complex marine system such

as the La Parguera (see review by Morse et al., 2007). Finally, it should be remembered that saturation state is fundamentally related to the free energy of the system to drive the reaction which can be capitalized by marine organisms. While corals have evolved a range of mechanisms to induce calcification (at least adult life stages), these are energy intensive processes having to overcome the kinetic barriers to calcification. The less free energy available in the ambient environment to drive reaction, the more energy corals will need to utilize for calcification.

The annual median free energy available to drive mineral precipitation for this Caribbean system are given in Table 3. On the La Parguera shelf reef system, net dissolution would be favored for Mg-calcite with >28 mol % $MgCO_3$. It is important to consider that the free energies shown here are based on solubilities for synthetic mineral phases while biogenic phases are considerably more soluble (Busenberg and Plummer, 1989). This would imply that the "true" free energies may be only a fifth that derived here owing to their distinct differences in physical properties, composition, structure, and reactivity relative to synthetic phases which are commonly assumed (Morse et al., 2007).

Adult marine calcifiers deploy a range of strategies to overcome this inhibition and drive the reaction at rates that often depart significantly from abiotic processes. However, the initial energy available to drive the reaction is reflected in the free energy pool of the ambient seawater. Whatever energy deficit may exist between the ambient pool and that needed to induce nucleation is energy that the organism must contribute itself. Due to the seasonal dynamics in free energy at Enrique reef, a coral must contribute an additional ~ 85 cal mol^{-1} $CaCO_3$ in the late fall relative to the spring regardless of the mineral phase being considered (Fig. 10).

This seasonal dynamic is relatively minor in comparison with the loss of the free energy that has been depleted from the system due to OA since the pre-industrial period, which has likely been greater than 155 cal mol^{-1} $CaCO_3$. By the end of the century under business-as-usual we can expect a loss ~337 cal mol^{-1} with respect to pre-industrial values, which will need to be compensated for by marine calcifiers in this system if they are going to maintain calcification.

Biogeosciences Discuss., https://doi.org/10.5194/bg-2018-408
Manuscript under review for journal Biogeosciences
Discussion started: 12 October 2018

5 Conclusions

Net heterotrophy and net dissolution dominate over most of the year on the Enrique forereef and off-reef areas while net autotrophic conditions coupled with calcification dominated from only January to mid-April (winter). The seasonal hysteresis between NEC and Ω_{arag} suggest that Ω_{arag} is not the main driver of NEC at the site. The NEC dynamics are mainly controlled by NEP and SST and reflect the combination of the biogeochemical and hydrodynamic processes on the reef shelf from the open ocean waters. This carbon subsidy likely originated from nearby mangroves and autochthonous benthic processes with much of the dissolution generated within the sediments and reef framework. The Enrique forereef serves as a continuous net source of CO_2 to the atmosphere. This is largely driven by the seasonal cycle of SST. The thermodynamics and metabolic activity are the dominant processes influencing the $pCO_{2,sw}$ changes at Enrique forereef, with air-sea CO_2 gas exchange and advective processes having minor impacts on the carbonate chemistry over the 2009 - 2017 period.

Constraining the local near-reef variability in carbonate chemistry across diel, seasonal, and annual scales is an important step in determining potential biogeochemical thresholds to OA for specific reef environments. At seasonal timescales, the Enrique net reef community metabolism may also affect the reef's susceptibility to pressures from OA. It is likely that Enrique Reef and other nearby reefs in La Parguera are already experiencing prolonged periods of net dissolution driven by high respiration rates. Future projections of the net erosional processes (chemical and biological) can be anticipated, assuming that surface waters continue to increase in accordance with current trends in CO_2 and temperature. While these waters will remain supersaturated with respect to aragonite for at least several centuries, the most soluble carbonate mineral forms such as 14 mol % $MgCO_3$, found in Enrique sediments and the marine lithified (cements) in the coral reef framework, are likely to experience prolonged undersaturation on an annual basis. This also have implications on the coral energy required to maintain active calcification during periods of low free energy. Based on similarities in environmental characteristics, our results suggest that tropical Caribbean reef ecosystems are exhibiting periods of net dissolution.

Our results demonstrate that current sustained high temporal robust autonomous capabilities of buoyed operational systems such as the La Parguera MapCO_2 buoy can be used to detect metabolic processes sensitive to OA. Future research efforts should be directed to combine different techniques and *in situ* methods for model validation in order to gain a better understanding of ecosystem changes across different temporal scales. Our methods yield a valuable index of cumulative net ecosystem effects of the biological processes affecting the water column over the reef. It is also important to note that we use data from fixed assets and that the methods may be scaled wherever similar data streams are found. Such results can be used to establish critical baselines against which future comparisons can be made, thus enabling evaluation of coral reef health and changes attributable to multiple stressors including OA. Further, high frequency data provided by this and similar operational systems can be used to develop early warning capabilities needed to identify and predict ecological community changes.

Data availability

The CO_2 buoy data are archived on the Ocean Carbon Data System (OCADS) at https://www.nodc.noaa.gov/ocads/data/0117354.xml; Sutton et al., (2014b).

The data from the ICON station is archived on National Centers for Environmental Information (NCEI) at https://www.nodc.noaa.gov/archive/arc0072/0124000/1.1/data/1-data/icon-lppr1-2013-data.csv; Hendee (2014).

The discrete data are archived on the NCEI at http://www.nodc.noaa.gov/oceanacidification/data/0145164.xml; Melendez et al. (2016).

The benthic community cover data are archived on the NCEI at https://data.nodc.noaa.gov/cgi-bin/iso?id=gov.noaa.nodc:0157740; Manzello et al. (2017).

Competing interests

The authors declare that they have no conflict of interest.

Acknowledgements

Support for this study was provided by the NOAA's Coral Reef Conservation Program through its AOAT project and the Ocean Acidification Program (OAP). UPRM participation in the latter is made possible through the IOOS partnership with CARICOOS program. We would like to give special thanks to Dr. Jorge Corredor for the opportunity of working with him and his work throughout the development of the AOAT. We also thank the staff and students of the UPRM Marine Sciences Department and UNH for field and lab assistance. We thank Helena Antoun, Belitza Brocco, Val Hensley and Erick García from UPRM for the assistance provided with the field and laboratory samples. We would like to thank Alyson Venti for providing the Be-7 sampling and residence time analyses. The authors are grateful for the constructive comments from Chris Hunt and Tyler Winsor. PMEL contribution number 4830.

References

Albright, R. and Mason, B.: Projected Near-Future Levels of Temperature and pCO2 Reduce Coral Fertilization Success, PLoS One, 8(2), 1–8, doi:10.1371/journal.pone.0056468, 2013.

Albright, R. A., Mason, B., Miller, M., and Langdon, C.: Ocean acidification compromises recruitment success of the threatened Caribbean coral, Acropora palmata, Proc. Natl. Acad. Sci. U.S.A., 107, 20400-20404, 2010.

Andersson, A. J., and Gledhill, D.: Ocean acidification and coral reefs: effects on breakdown, dissolution, and net ecosystem calcification, Ann. Rev. Mar. Sci., 5, 321–48, doi:10.1146/annurev-marine-121211-172241, 2013.

Andersson, A. J., Kuffner, I. B., Mackenzie, F. T., Jokiel, P. L., Rodgers, K. S., and Tan, A.: Net loss of $CaCO_3$ from coral reef communities due to human induced seawater acidification, Biogeosciences Discuss., 6(1), 2163–2182, doi:10.5194/bgd-6-2163-2009, 2009.

Anthony, K. R. N., Kline, D. I., Diaz-Pulido, G., Dove, S., and Hoegh-Guldberg, O.: Ocean acidification causes bleaching and productivity loss in coral reef builders, Proc. Natl. Acad. Sci. U.S.A., 105(45), 17442–6, doi:10.1073/pnas.0804478105, 2008.

Appeldoorn, R.S., Yoshioka, P.M., and Ballantine, D.L.: Coral reef ecosystem studies: Integrating science and management in the Caribbean, Caribb. J. Sci., 45(2–3),134-137, 2009.

Ballantine, D.L., Appeldoorn, R.S., Yoshioka, P., Weil, E., Armstrong, R., Garcia, J.R., Otero, E., Pagan, F., Sherman, C., Hernandez-Delgado, E.A., Bruckner, A., and Lilyestrom, C.: Biology and Ecology of Puerto Rican Coral Reefs, In Riegl BM, Dodge RE (eds) Coral Reefs of the USA. Springer, Berlin, 375-406, 2008.

Bates, N. R., Amat, A., and Andersson, A. J.: Feedbacks and responses of coral calcification on the Bermuda reef system to seasonal changes in biological processes and ocean acidification, Biogeosciences, 7(8), 2509–2530, doi:10.5194/bg-7-2509-2010, 2010.

Bates, N. R., Amat, A. and Andersson, A. J.: The interaction of ocean acidification and carbonate chemistry on coral reef calcification: evaluating the carbonate chemistry Coral Reef Ecosystem Feedback (CREF) hypothesis on the Bermuda coral reef, Biogeosciences Discuss., 6(4), 7627–7672, doi:10.5194/bgd-6-7627-2009, 2009.

Bates, N. R.: Seasonal variability of the effect of coral reefs on seawater CO_2 and air-sea CO_2 exchange, Limnol. Oceanogr., 47(1), 43–52, doi:10.4319/lo.2002.47.1.0043, 2002.

Bates, N. R., Best, M. H. P., Neely, K., Garley, R., Dickson, A. G., and Johnson, R. J.: Detecting anthropogenic carbon dioxide uptake and ocean acidification in the North Atlantic Ocean, Biogeosciences, 9(7), 2509–2522, doi:10.5194/bg-9-2509-2012, 2012.

Bates, N. R.: Twenty Years of Marine Carbon Cycle Observations at Devils Hole Bermuda Provide Insights into Seasonal Hypoxia, Coral Reef Calcification, and Ocean Acidification, Front. Mar. Sci., 4, 1–23, doi:10.3389/fmars.2017.00036, 2017.

Borowitzka, M. A.: Photosynthesis and calcification in the articulated coralline red algae Amphiroa anceps and A. foliacea, Mar. Biol., 62, 17–23, 1981.

Boucher, G., Clavier, J., Hily, C. and Gattuso, J.-P.: Contribution of soft-bottoms to the community metabolism (primary production and calcification) of a barrier reef flat (Moorea, French Polynesia), J. Exp. Mar. Bio. Ecol., 225(2), 269–283, doi:10.1016/S0022-0981(97)00227-X, 1998.

Busenberg, E. and Plummer, L. N.: Thermodynamics of magnesian calcite solid-solutions at 25 ◦C and 1 atm total pressure, Geochim. Cosmochim. Ac., 53, 1189–1208, 1989.

Cao, L., and Caldeira, K.: Atmospheric CO_2 stabilization and ocean acidification, Geophys. Res. Lett., 35(19), 1–5, doi:10.1029/2008GL035072, 2008.

Chan, N. C. S., and Connolly, S. R.: Sensitivity of coral calcification to ocean acidification: a meta–analysis. Glob. Chang. Biol. 19, 282–290, doi: 10.1111/gcb.12011, 2013.

Cohen, A. L. L. and Holcomb, M.: Why corals care about ocean acidification: Uncovering the mechanism, Oceanography, 22(4), 118–127, 2009.

Comeau, S., Lantz, C. A., Edmunds, P. J., and Carpenter, R. C.: Framework of barrier reefs threatened by ocean acidification, Glob. Chang. Biol., 22(3), doi:10.1111/gcb.13023, 2016.

Conway, T. J., Tans, P. P., Waterman, L. S., Thoning, K. W., Kitzis, D. R., Masarie, K. A., and Zhang, N.: Evidence for interannual Variability of the carbon cycle from the National Oceanic and Atmospheric Administration/Climate Monitoring and Diagnostics Laboratory global air sampling network, J. Geophys. Res., 99, 22831-22855,1994.

Corredor, J. E., and Morell, J. M.: Seasonal variation of physical and biogeochemical features in eastern Caribbean Surface Water, J. Geophys. Res., 106(C3), 4517– 4525, doi:10.1029/2000JC000291, 2001.

Courtney, T. A., Andersson, A. J., Bates, N. R., Collins, A., Cyronak, T., de Putron, S. J., Eyre, B. D., Garley, R., Hochberg, E. J., Johnson, R., Musielewicz, S., Noyes, T. J., Sabine, C. L., Sutton, A. J., Toncin, J., and Tribollet, A.: Comparing Chemistry and Census-Based Estimates of Net Ecosystem Calcification on a Rim Reef in Bermuda, Front. Mar. Sci., 3, 181, doi:10.3389/fmars.2016.00181, 2016.

Cyronak, T., Andersson, A. J., Langdon, C., Albright, R., Bates, N. R., Caldeira, K., Carlton, R., Corredor, J. E., Dunbar, R. B., Enochs, I., Erez, J., Eyre, B. D., Gattuso, J.-P., Gledhill, D., Kayanne, H., Kline, D. I., Koweek, D. A., Lantz, C., Lazar, B., Manzello, D., McMahon, A., Meléndez, M., Page, H. N., Santos, I. R., Schulz, K. G., Shaw, E., Silverman, J., Suzuki, A., Teneva, L., Watanabe, A., and Yamamoto, S.: Taking the metabolic pulse of the world's coral reefs, PLoS One, 13(1), e0190872, 2018.

Dickson, A. G.: Thermodynamics of the dissociation of boric acid in potassium chloride solutions from 273.15 to 318.15 K, J. Chem. Eng. Data., 35(3), 253–257, 1990.

Dickson, A. G., Sabine, C. L., and Christian, J. R.: Guide to best practices for ocean CO_2 measurements. Sidney, British Columbia, North Pacific Marine Science Organization, PICES Special Publication 3, 2007.

Doropoulos, C., Ward, S., Diaz-Pulido, G., Hoegh-Guldberg, O., Mumby, P.J.: Ocean acidification reduces coral recruitment by disrupting intimate larval-algal settlement interactions, Ecology Letters, 15, 338–346, 2012.

Duarte, C. M., Hendriks, I. E., Moore, T. S., Olsen, Y. S., Steckbauer, A., Ramajo, L., Carstensen, J., Trotter, J. A., and McCulloch, M.: Is Ocean Acidification an Open-Ocean Syndrome? Understanding Anthropogenic Impacts on Seawater pH, Estuaries and Coasts, 36(2), 221–236, doi:10.1007/s12237-013-9594-3, 2013.

Eyre, B. D., Andersson, A. J., and Cyronak, T.: Benthic coral reef calcium carbonate dissolution in an acidifying ocean, Nat. Clim. Chang., 4(11), 969–976, doi:10.1038/nclimate2380, 2014.

Eyre, B. D., Cyronak, T., Drupp, P., Carlo, E. H. De, Sachs, J. P., and Andersson, A. J.: Dissolving Before End of Century, 911, 908–911, doi:10.1126/science.aao1118, 2018.

Falter, J. L., Lowe, R. J., Atkinson, M. J., Monismith, S. G., and Schar, D. W.: Continuous measurements of net production over a shallow reef community using a modified Eulerian approach, J. Geophys. Res., 113(C7), C07035, doi:10.1029/2007JC004663, 2008.

Falter, J. L., Lowe, R. J., Zhang, Z., and McCulloch, M.: Physical and biological controls on the carbonate chemistry of coral reef waters: effects of metabolism, wave forcing, sea level, and geomorphology, PLoS One, 8(1), e53303, doi:10.1371/journal.pone.0053303, 2013.

Fassbender, A. J., Sabine, C. L., and Feifel, K. M.: Consideration of coastal carbonate chemistry in understanding biological calcification, 43(9), 4467-4476, doi:10.1002/2016GL068860, 2016.

Friedrich, T., Timmermann, a, Abe-Ouchi, a, Bates, N. R., Chikamoto, M. O., Church, M. J., Dore, J. E., Gledhill, D. K., González-Dávila, M., Heinemann, M., Ilyina, T., Jungclaus, J. H., McLeod, E., Mouchet, a and

957 Santana-Casiano, J. M.: Detecting regional anthropogenic trends in ocean acidification against natural variability,
958 Nat. Clim. Chang., 2(3), 167–171, doi:10.1038/nclimate1372, 2012.
959
960 Gao, K., Aruga, Y., Asada, K., Ishihara, T., Akano, T., and Kiyohara, M.: Calcification in the articulated
961 coralline alga Coralline pilulifera, with special reference to the effect of elevated CO_2 concentration, Mar. Biol.,
962 117, 129–132, 1993.
963
964 García, H. E., and Gordon, L. I.: Oxygen solubility in seawater: Better fitting equations, Limnol. Oceanogr.,
965 37(6), 1307–1312, doi:10.4319/lo.1992.37.6.1307, 1992.
966
967 Gardner, T. A., Cote, I. M., Gill, J. A., Grant, A. and Watkinson, A. R.: Long-Term Region-Wide Declines in
968 Caribbean Corals, Science, 301(5635), 958–960, doi:10.1038/020493a0, 2003.
969
970 García-Sais, J., Appeldoorn, R., Battista, T., Bauer, L., Bruckner, A., Caldow, C., Carrubba, L., Corredor, J.,
971 Diaz, E., Lilyestrom, C., and García-Moliner, G.: The state of coral reef ecosystems of Puerto Rico,The state of
972 coral reef ecosystems of the United States and Pacific Freely Associated States, 1, 2008.
973
974 Gattuso, J. P., Frankignoulle, M., Bourge, I., Romaine, S., and Buddemeier, R. W.: Effect of calcium carbonate
975 saturation of seawater on coral calcification, Glob. Planet. Change, 18(1–2), 37–46, doi:10.1016/S0921-
976 8181(98)00035-6, 1998.
977
978 Gattuso, J. P., Pichon, M., Delesalle, B., Canon, C., and Frankignoulle, M.: Carbon fluxes in coral reefs. I.
979 Lagrangian measurements of community metabolism and resulting air-sea CO_2 disequilibrium, Mar. Ecol. Prog.
980 Ser., 145, 109–121, 1996.
981
982 Gledhill, D. K., Wanninkhof, R., Millero, F. J., and Eakin, M.: Ocean acidification of the Greater Caribbean
983 Region 1996–2006, J. Geophys. Res., 113(C10031), 1–11, doi:10.1029/2007JC004629, 2008.
984
985 Glynn, P. W., and Manzello, D. P.: Bioerosion and Coral Reef Growth: A Dynamic Balance. in: Birkeland C.
986 (eds), Coral Reefs in the Anthropocene, Springer, Dordrecht, 67-97, https://doi.org/10.1007/978-94-017-7249-
987 5_4, 2015.
988
989 Gratwicke, B., and Speight, M. R.: Effects of habitat complexity on Caribbean marine fish assemblages, Mar.
990 Ecol. Prog. Ser., 292, 301–310, doi:10.3354/meps292301, 2005
991
992 Gray, S. E. C., DeGrandpre, M. D., Langdon, C., and Corredor, J.E.: Short-term and seasonal pH, pCO2 and
993 saturation state vari- ability in a coral-reef ecosystem, Global Biogeochem. Cy., 26, GB3012,
994 doi:10.1029/2011gb004114, 2012.
995
996 Gruber, N., C. D. Keeling, and T. F. Stocker (1998), Carbon-13 constraints on the seasonal inorganic carbon
997 budget at the BATS site in the northwestern Sargasso Sea, Deep Sea Res., I, 45, 673–717.
998
999 Guinotte, J.M., Buddemeier, R.W., Kleypas, J.A.: Future coral reef habitat marginality: temporal and spatial
000 effects of climate change in the Pacific basin. Coral Reefs 22, 551–558, 2003.

001 Hendee, James C.; US DOC/NOAA/OAR > Atlantic Oceanographic and Meteorological Laboratory (2014).

Integrated Coral Observing Network (ICON) - Media Luna Reef (LPPR1 - La Parquera Natural Reserve, Puerto Rico) Meteorological and Oceanographic Observations from 2013-01-01 to 2013-03-20 (NODC Accession 0124000). Version 1.1. National Oceanographic Data Center, NOAA. Dataset.

Hernández, R., Sherman, C., Weil, E., and Yoshioka, P.: Spatial and temporal patterns in reef sediment accumulation and composition, southwestern insular shelf of Puerto Rico, Caribb. J. Sci., 45(2–3), 138–150, 2009.

Hsu, S. A., Meindl, E. A. and Gilhousen, D. B.: Determining the Power-Law Wind-Profile Exponent under Near-Neutral Stability Conditions at Sea, J. Appl. Meteorol., 33(6), 757–765, doi:10.1175/1520-0450(1994)033<0757:DTPLWP>2.0.CO;2, 1994.

IPCC: Climate Change 2014: Synthesis Report. Contribution of Working Groups I, II and III to the Fifth Assessment Report of the Intergovernmental Panel on Climate Change. Core Writing Team, R.K. Pachauri and L.A. Meyer (eds) Geneva, Switzerland, 151, 2014.

Jiang, L.-Q., Cai, W.-J. W.-J., Wanninkhof, R., Wang, Y. and Lüger, H.: Air-sea CO2 fluxes on the U.S. South Atlantic Bight: Spatial and seasonal variability, J. Geophys. Res., 113(C7), 1–17, doi:10.1029/2007jc004366, 2008.

Kinsey, D.W.: Metabolism, calcification and carbon production. I. System Level Studies. Proceedings of the 5th International Coral Reef Congress, Tahiti, 22, 1985.

Kleypas, J. A., Buddemeier, R. W., Archer, D., Gattuso, J. P., Langdon, C., and Opdyke, B. N.: Geochemical consequences of increased atmospheric carbon dioxide on coral reefs, Science, 284,118–-120, 1999.

Langdon, C., and Atkinson, M. J.: Effect of elevated pCO_2 on photosynthesis and calcification of corals and interactions with seasonal change in temperature/irradiance and nutrient enrichment, J. Geophys. Res. Ocean., 110(C9), 1–16, doi:10.1029/2004JC002576, 2005.

Langdon, C., Takahashi, T., Sweeney, C., Chipman, D., Goddard, J., Marubini, F., Aceves, H., Barnett, H., and Atkinson, M.: Effect of calcium carbonate saturation state on the calcification rate of an experimental coral reef, Global Biogeochem. Cycles, 14(2), 639–654, 2000.

Langdon, C., Broecker, W. S., Hammond, D. E., Glenn, E., Fitzsimmons, K., Nelson, S. G., Peng, T.-H., Hajdas, I., and Bonani, G.: Effect of elevated CO2 on the community metabolism of an experimental coral reef, Global Biogeochem. Cycles, 17(1), doi:10.1029/2002GB001941, 2003.

Le Quéré, C., Andrew, R. M., Canadell, J. G., Sitch, S., Ivar Korsbakken, J., Peters, G. P., Manning, A. C., Boden, T. A., Tans, P. P., Houghton, R. A., Keeling, R. F., Alin, S., Andrews, O. D., Anthoni, P., Barbero, L., Bopp, L., Chevallier, F., Chini, L. P., Ciais, P., Currie, K., Delire, C., Doney, S. C., Friedlingstein, P., Gkritzalis, T., Harris, I., Hauck, J., Haverd, V., Hoppema, M., Klein Goldewijk, K., Jain, A. K., Kato, E., Körtzinger, A., Landschützer, P., Lefèvre, N., Lenton, A., Lienert, S., Lombardozzi, D., Melton, J. R., Metzl, N., Millero, F., Monteiro, P. M. S., Munro, D. R., Nabel, J. E. M. S., Nakaoka, S. I., O'Brien, K., Olsen, A., Omar, A. M., Ono, T., Pierrot, D., Poulter, B., Rödenbeck, C., Salisbury, J., Schuster, U., Schwinger, J., Séférian, R., Skjelvan, I., Stocker, B. D., Sutton, A. J., Takahashi, T., Tian, H., Tilbrook, B., Van Der Laan-Luijkx, I. T., Van Der Werf, G.

R., Viovy, N., Walker, A. P., Wiltshire, A. J. and Zaehle, S.: Global Carbon Budget 2016, Earth Syst. Sci. Data, 8(2), 605–649, doi:10.5194/essd-8-605-2016, 2016.

Leclercq, N., Gattuso, J. P., and Jaubert, J.E.A.N.: CO_2 partial pressure controls the calcification rate of a coral community, Glob. Chang. Biol., 6(3), 329–334, doi:10.1046/j.1365-2486.2000.00315.x, 2000.

Leclercq, N., Gattuso, J. P., and Jaubert, J.: Primary production, respiration and calcification of a coral reef mesocosm under increased CO_2 partial pressure, Limnol. Oceanogr., 47(2), 558– 564, 2002.

Lee, K., Choi, S. D., Park, G. H., Wanninkhof, R., Peng, T. H., Key, R. M., Sabine, C. L., Feely, R. A., Bullister, J. L., Millero, F. J., and Kozyr, A.: An updated anthropogenic CO_2 inventory in the Atlantic Ocean, Global Biogeochem. Cy., 17(4), 1116, doi:10.1029/2003GB002067, 2003.

Lee, K., Tong, L. T., Millero, F. J., Sabine, C. L., Dickson, A. G., Goyet, C., Park, G.-H. H., Wanninkhof, R., Feely, R. A., and Key, R. M.: Global relationships of total alkalinity with salinity and temperature in surface waters of the world's oceans, Geophys. Res. Lett., 33(19), 1–5, doi:10.1029/2006GL027207, 2006.

Lowe, R. J., Falter, J. L., Monismith, S. G., and Atkinson, M. J.: A numerical study of circulation in a coastal reef-lagoon system, J. Geophys. Res. Ocean., 114(6), 873–893, doi:10.1029/2008JC005081, 2009.

Lueker, T. J., Dickson, A. G. and Keeling, C. D.: Ocean pCO2 calculated from dissolved inorganic carbon, alkalinity, and equations for K1 and K2: validation based on laboratory measurements of CO2 in gas and seawater at equilibrium, Mar. Chem., 70(1), 105–119, doi:https://doi.org/10.1016/S0304-4203(00)00022-0, 2000.

Lugo-Fernández, A., Roberts, H. H., and Suhayda, J. N.: Wave transformations across a Caribbean fringing-barrier Coral Reef, Cont. Shelf Res., 18(10), 1099–1124, doi:10.1016/S0278-4343(97)00020-4, 1998.

Manning, C. C., and Nicholson, D. P.: Gas_toolbox: MATLAB code used in Manning et al. GTWS-7 proceedings. Zenodo. DOI: 10.5281/zenodo.45293, 2016.

Manzello, D., Enochs, I., Valentino, L., Kolodziej, G., Carlton, R., Jones, P.: National Oceanic and Atmospheric Administration; Cooperative Institute for Marine and Atmospheric Studies. National Coral Reef Monitoring Program: Carbonate Budget data of Cayo Enrique near La Parguera, Puerto Rico from 2015-08-03 to 2015-08-07 (NCEI Accession 0157740). Version 1.1. NOAA National Centers for Environmental Information. Dataset, 2017.

Marshall, A. T., and Clode, P. L.: Effect of increased calcium concentration in sea water on calcification and photosynthesis in the scleractinian coral Galaxea fascicularis, J. Exp. Biol., 205, 2107–2113, 2002.

Marubini, F., Barnett, H., Langdon, C., and Atkinson, M.: Dependence of calcification on light and carbonate ion concentration for the hermatypic coral Porites compressa, Mar. Ecol. Prog. Ser., 220, 153–162, doi:10.3354/meps220153, 2001.

Masarie, K. A., and Tans, P. P.: Extension and integration of atmospheric carbon dioxide data into a globally consistent measurement record, J. Geophys. Res.-Atmos., 100, 11593–11610, 1995.

McGillis, W. R., Langdon, C., Williams, A. J. and Loose, B.: O2 -MAVS: an Instrument for Measuring Oxygen Flux, in OCEANS 2009, pp. 1–9., doi:10.23919/OCEANS.2009.5422166, 2009.

McGillis, W. R., Langdon, C., Loose, B., Yates, K. K., and Corredor, J. E.: Productivity of a coral reef using boundary layer and enclosure methods, Geophys. Res. Lett., 38(3), 2–6, doi:10.1029/2010GL046179, 2011.

Morelock, J., Schneidermann, N., and Bryant, W. R.: Shelf reefs, southwestern Puerto Rico, Stud. Geol., 4, 17–25, 1977.

Morelock, J., Ramirez, W. R., Bruckner, A. W., and Carlo, M.: Status of coral reefs, southwest Puerto Rico, Caribb. J. Sci. Spec. Publ., 4, 1–57, 2001.

Morse, J. W. and Arvidson, R. S.: The dissolution kinetics of major sedimentary carbonate minerals, Earth-Science Rev., 58(1–2), 51–84, doi:10.1016/S0012-8252(01)00083-6, 2002.

Morse, J. W., Arvidson, R. S. and Lüttge, A.: Calcium carbonate formation and dissolution, Chem. Rev., doi:10.1021/cr050358j, 2007.

Morse, J. W., and Mackenzie, F. T.: Geochemistry of Sedimentary Carbonates, Elsevier B.V., 1990.

Moyer, R. P., Viehman, T. S., Piniak, G. A., and Gledhill, D. K.: Linking seasonal changes in benthic community structure to seawater chemistry, In Proceedings, 12th International Coral Reef Symposium. Cairns, Australia, 2012.

Mucci, A.: The solubility of Calcite and Aragonite in Seawater at various Salinities, Temperatures, and one Atmosphere Total Pressure, Am. J. Sci., 283, 780–799, 1983.

Muehllehner, N., Langdon, C., Venti, A., and Kadko, D.: Dynamics of carbonate chemistry, production, and calcification of the Florida Reef Tract (2009–2010): Evidence for seasonal dissolution, Global Biogeochemical Cycles, 30, 661–688, doi:10.1002/2015GB005327, 2016.

Ohde, S., and Hossain, M. M. M.: Effect of $CaCO_3$ (aragonite) saturation state of seawater on calcification of Porites coral, Geochemical Journal, 38(6), 613-621, 2004.

Otero, E. and Carbery, K. K.: Chlorophyll a and turbidity patterns over coral reefs systems of La Parguera Natural Reserve, Puerto Rico, Rev. Biol. Trop., 53(SUPPL. 1), 25–32, 2005.

Page, H. N., Courtney, T. A., Collins, A., De Carlo, E. H., and Andersson, A. J.: Net Community Metabolism and Seawater Carbonate Chemistry Scale Non-intuitively with Coral Cover, Front. Mar. Sci., doi:10.3389/fmars.2017.00161, 2017.

Perry, C. T., Steneck, R. S., Murphy, G. N., Kench, P. S., Edinger, E. N., Smithers, S. G., and Mumby, P. J., Regional-scale dominance of non-framework building corals on Caribbean reefs affects carbonate production and future reef growth. Global change biology, 21(3),1153-1164, 2015.

Perry, C. T., Murphy, G. N., Kench, P. S., Smithers, S. G., Edinger, E. N., Steneck, R. S., and Mumby, P. J.: Caribbean-wide decline in carbonate production threatens coral reef growth, Nat. Commun., 4, 1402, doi:10.1038/ncomms2409, 2013.

Perry, C. T., Alvarez-Filip, L., Graham, N. A. J., Mumby, P. J., Wilson, S. K., Kench, P. S., Manzello, D. P., Morgan, K. M., Slangen, A. B. A., Thomson, D. P., Januchowski-Hartley, F., Smithers, S. G., Steneck, R. S., Carlton, R., Edinger, E. N., Enochs, I. C., Estrada-Saldívar, N., Haywood, M. D. E., Kolodziej, G., Murphy, G. N., Pérez-Cervantes, E., Suchley, A., Valentino, L., Boenish, R., Wilson, M. and Macdonald, C.: Loss of coral reef growth capacity to track future increases in sea level, Nature, 558(7710), 396–400, doi:10.1038/s41586-018-0194-z, 2018.

Pittman, S. J., Hile, S. D., Jeffrey, C. F. G., Clark, R., Woody, K., Herlach, B. D., Caldow, C., Monaco, M., and Appeldoorn, R. S.: Coral reef ecosystems of Reserva Natural de La Parguera (Puerto Rico): Spatial and temporal patterns in fish and benthic communities (2001-2007), NOAA Tech. Mem. NOS NCCOS 107, 202, 2010.

Plummer, L. N., Wigley, T. M. L., and Parkhurst D. L.: The kinetics of calcite dissolution in CO2-water systems at 5 to 60 °C and 0.0 to 1.0 atm CO2. Amer. Jour. Sci. 278, 179-216, 1978.

Revelle, R., and Suess, H. E.: Carbon dioxide exchange between atmosphere and ocean and the question of an increase of atmospheric CO_2 during the past decades, Tellus, 9, 18–27, 1957.

Ricke, K. L., Orr, J. C., Schneider, K., and Caldeira, K.: Ricks to coral reefs from ocean carbonate chemistry changes in recent earth system model projections, Environ. Res. Lett., 8, 1–6, doi:10.1088/1748-9326/8/3/034003, 2013.

Riebesell, U., Zondervan, I., Rost, B., Tortell, P. D., Zeebe, R. E., and Morel, F. M.: Reduced calcification of marine plankton in response to increased atmospheric CO_2, Nature, 407(6802), 364–7, doi:10.1038/35030078, 2000.

Ryan, K. E., Walsh, J. P., Corbett, D. R., and Winter, A.: A record of recent change in terrestrial sedimentation in a coral-reef environment, La Parguera, Puerto Rico: A response to coastal development?, Mar. Pollut. Bull., doi:10.1016/j.marpolbul.2008.02.017, 2008.

Sabine, C. L., Feely, R. A., Gruber, N., Key, R. M., Lee, K., Bullister, J. L., Wanninkhof, R., Wong, C. S., Wallace, D. W. R., Tilbrook, B., Millero, F. J., Peng, T.-H., Kozyr, A., Ono, T., and Rios, A. F.: The oceanic sink for anthropogenic CO_2, Science, 305(5682), 367–71, doi:10.1126/science.1097403, 2004.

Shadwick, E. H., Thomas, H., Azetsu-Scott, K., Greenan, B. J. W., Head, E., and Horne, E.: Seasonal variability of dissolved inorganic carbon and surface water pCO_2 in the Scotian Shelf region of the Northwestern Atlantic, Mar. Chem., 124, 23–37, doi:10.1016/j.marchem.2010.11.004, 2011.

Shamberger, K. E. F., Feely, R. A., Sabine, C. L., Atkinson, M. J., DeCarlo, E. H., Mackenzie, F. T., Drupp, P. S., and Butterfield, D. A.: Calcification and organic production on a Hawaiian coral reef, Mar. Chem., 127, 64–75, doi:10.1016/j.marchem.2011.08.003, 2011.

Silbiger, N. J., Guadayol, Ò., Thomas, F. I. M., and Donahue, M. J.: Reefs shift from net accretion to net erosion along a natural environmental gradient, Mar. Ecol. Prog. Ser., 515, 33–44, doi:10.3354/meps10999, 2014.

Silverman, J., Lazar, B., and Erez, J.: Effect of aragonite saturation, temperature, and nutrients on the community calcification rate of a coral reef, J. Geophys. Res.-Oceans, 112, doi:10.1029/2006JC003770, 2007.

Smith, S. V., and Jokiel, P. L.: Water composition and biogeochemical gradients in the Canton Atoll lagoon. Atoll Res. Bull., 221,15-53,1978.

Stearn, C. W., Scoffin, T. P., and Martinade, W.: Calcium carbonate budget of a fringing reef on the west coast of Barbados Part 1 – zonation and productivity, J. Mar. Sci., 27, 479–510, 1977.

Strickland, J. D., and Parsons, T. R.: A practical handbook of seawater analysis, 1972.

Sutton, A. J., Sabine, C. L., Maenner-Jones, S., Lawrence-Slavas, N., Meinig, C., Feely, R. A., Mathis, J. T., Musielewicz, S., Bott, R., McLain, P. D., Fought, H. J., and Kozyr, A.: CDIAC data management and archival support for a high-frequency atmospheric and seawater pCO_2 data set from 14 open ocean moorings, Earth Syst. Sci. Data, 6, 353–366, doi:10.3334/CDIAC/OTG.TSM, 2014a.

Sutton, A. J., Sabine, C. L., Morell, J. M., Musielewicz, S., Maenner, S., Dietrich, C., Bott, R., Osborne, J.: High-resolution ocean and atmosphere pCO_2 time-series measurements from mooring La_Parguera_67W_18N in the Caribbean Sea: NODC Accession 0117354. Version 5.5. National Oceanographic Data Center, NOAA. Dataset. doi:10.3334/CDIAC/OTG.TSM_LA_PARGUERA_67W_18N, 2014b.

Takahashi, T., Olafsson, J., Goddard, J. G., Chipman, D. W., and Sutherland, S. C.: Seasonal variation of CO_2 and nutrients in the high-latitude surface oceans: A comparative study. Global Biogeochemical Cycles, 7(4), 843-878, 1993.

Takeshita, Y., McGillis, W., Briggs, E. M., Carter, A. L., Donham, E. M., Martz, T. R., Price, N. N., and Smith, J. E.: Journal of Geophysical Research: Oceans coral reef using a boundary layer approach, 5655–5671, doi:10.1002/2016JC011886, 2016.

Teneva, L., Dunbar, R. B., Mucciarone, D. A., Dunckley, J. F., and Koseff, J. R.: High-resolution carbon budgets on a Palau back-reef modulated by interactions between hydrodynamics and reef metabolism, Limnol. Oceanogr., 58, doi:10.4319/lo.2013.58.5.1851, 2013.

Turk, D., Yates, K. K., Vega-Rodriguez, M., Toro-Farmer, G., L'Esperance, C., Melo, N., Ramsewak, D., Dowd, M., Estrada, S. C., Muller-Karger, F. E., Herwitz, S. R., and McGillis, W. R.: Community metabolism in shallow coral reef and seagrass ecosystems, lower Florida Keys, Mar. Ecol. Prog. Ser., 538, 35–52, doi:10.3354/meps11385, 2015.

van Heuven, S., Pierrot, D., Rae, J.W.B., Lewis, E., and Wallace, D.W.R.: MATLAB Program Developed for CO2 System Calculations. ORNL/CDIAC-105b. Carbon Dioxide Information Analysis Center, Oak Ridge National Laboratory, U.S. Department of Energy, Oak Ridge, Tennessee. doi: 10.3334/CDIAC/otg.CO2SYS_MATLAB_v1.1, 2011.

Venti, A., Andersson, A., and Langdon, C.: Multiple driving factors explain spatial and temporal variability in coral calcification rates on the Bermuda platform, Coral Reefs, 979–997, doi:10.1007/s00338-014-1191-9, 2014.

Venti, A., Kadko, D., Andersson, A.J., Langdon, C., and Bates, N. R.: A multi-tracer model approach to estimate reef water residence times. Limnology and Oceanography: Methods, 10(12),1078-1095, 2012.

Wanninkhof, R.: Relationship between wind speed and gas exchange over the ocean revisited, Limnol. Oceanogr. Methods, 12(6), 351–362, doi:10.4319/lom.2014.12.351, 2014.

Winkler, L.S.: The determination of dissolved oxygen. Ber. Dtsche. Chern. Ges., 21, 2843-2855, 1888

Weiss, R. F.: Carbon dioxide in water and seawater: the solubility of a non-ideal gas, Mar. Chem., 2, 203–215, 1974.

Xue, L., Cai, W. J., Hu, X., Sabine, C., Jones, S., Sutton, A. J., Jiang, L. Q., and Reimer, J. J.: Sea surface carbon dioxide at the Georgia time series site (2006-2007): Air-sea flux and controlling processes, Prog. Oceanogr., 140, 14–26, doi:10.1016/j.pocean.2015.09.008, 2016.

Yates, K. K., and Halley, R. B.: CO_3^{2-} concentration and pCO_2 thresholds for calcification and dissolution on the Molokai reef flat, Hawaii, Biogeosciences, 3(3), 357–369, 2006.

Yates, K. K., Halley, R. B., and Moomaw, A.: The Submersible Habitat for Analyzing Reef Quality (SHARQ): Improved technology for benthic analyses and experimentation, 28–30, 1999.

Yeakel, K. L., Andersson, A. J., Bates, N. R., Noyes, T. J., Collins, A., and Garley, R.: Shifts in coral reef biogeochemistry and resulting acidification linked to offshore productivity, Proc. Natl. Acad. Sci., 112(47), 14512–14517, doi:10.1073/pnas.1507021112, 2015.

Zayas-Santiago, C. C.: Landscape structure in two reefs in La Parguera and the distribution of the Lytechinus variegatus, University of Puerto Rico, Mayaguez Campus, 2011.

Zeebe, R. E., and Wolf-Gladrow, D. A.: CO2 in seawater: equilibrium, kinetics, isotopes, Gulf Professional Publishing,65, 2001.

Biogeosciences Discuss., https://doi.org/10.5194/bg-2018-408
Manuscript under review for journal Biogeosciences
Discussion started: 12 October 2018

Table 1: MapCO_2 observations and model uncertainties.

Buoy Observations	Error ±	Method
Temperature (°C)	± 0.01	Sutton et al. (2014a)
Salinity (SSS)	± 0.05	Sutton et al. (2014a)
pCO_{2sw} (µatm)	± <2	Sutton et al. (2014a)
O_2	± 3 %	See Section 2.3
Model parameter		
TA_{reef} (µmol kg^{-1})	± 16	Monte Carlo
DIC_{reef} (µmol kg^{-1})	± 12	Monte Carlo
Ω_{arag}	± 0.12	Monte Carlo
CO_2 Flux (mmol m^{-2} day^{-1})	± 0.72	Sum of the squares
O_2 Flux (mmol m^{-2} day^{-1})	± 2.04	Monte Carlo
$DIC_{AIR\text{-}SEA\ EX}$ (µmol kg^{-1})	± 0.24	Monte Carlo
DIC_{BIO} (mmol m^{-2})	± 0.3	Monte Carlo
Revelle Factor	± 0.66	Monte Carlo
$\partial pCO_{2,OBS}$ (µatm)	± 1.1	Monte Carlo
$\partial pCO_{2,SOL}$(µatm)	± 0.3	Monte Carlo
$\partial pCO_{2,AIR\text{-}SEA\ EX}$ (µatm)	± 0.1	Monte Carlo
$\partial pCO_{2,HOR\ MIX}$ (µatm)	± 0.5	Gradient observations*
$\partial pCO_{2,BIO}$ (µatm)	± 1.2	Monte Carlo
NEP (mmol C m^{-2} day^{-1})	± 2.08	Monte Carlo
NEC (mmol $CaCO_3$ m^{-2} day^{-1})	± 2.18	Monte Carlo

*refer to Sect. 2.6.2 for details

Biogeosciences Discuss., https://doi.org/10.5194/bg-2018-408
Manuscript under review for journal Biogeosciences
Discussion started: 12 October 2018

Table 2: Summary of the reef station seasonal variability of the carbonate and oceanography parameters from 2009 to 2017. The (±) is the standard deviation.

Parameter	Mean	Max	Min	Seasonal change
Temperature (˚C)	28.5 ± 0.41	30.2	26.6	3.62
Salinity	35.3 ± 0.26	36.1	34.4	1.63
Wind speed (m s^{-1})	4.21 ± 1.76	6.38	2.36	4.01
Residence Time (days)*	15 ± 3	9 ± 2 (Jan)	13 ± 2 (May)	4
DIC (µmol kg^{-1}_{sw})	1972 ± 13.9	2000	1931	69.3
TA (µmol kg^{-1}_{sw})	2287 ± 13.7	2332	2231	101
Revelle Factor	9.25 ± 0.11	9.49	9.06	0.43
$pCO_{2,sw}$ (µatm)	423 ± 13.5	461	387	73.1
$pCO_{2,air}$ (µatm)	386 ± 8.52	391	378	12.6
$\Delta pCO_{2,sea\text{-}air}$ (µatm)	38.2 ± 14.2	80.8	0.72	80.1
pH (total scale)	8.02 ± 0.01	8.06	7.98	0.07
Ω_{arag}	3.59 ± 0.07	3.76	3.4	0.36
O_2 (µmol kg^{-1})	176 ± 10.6	192	154	37.8
F_{CO2} (mmol m^{-2} day^{-1})	2.04 ± 2.13	6.78	0.11	6.67
F_{O2} (mmol m^{-2} day^{-1})	-23.3 ± 22.5	14.2	-86.6	72.4
NEC (mmol m^{-2} day^{-1})	-18.1 ± 2.1	12.0	-57.7	45.7
NEP (mmol m^{-2} day^{-1})	17.9 ± 2.2	66.8	-10.9	55.9

*Reef water residence time relative to the offshore station located ~11 km from Enrique reef (for details, see Sect. 2.2).

Table 3: Annual median Gibbs Free Energy (ΔG, cal mol^{-1} $CaCO_3$) for a range of $CaCO_3$ mineral phases under ambient conditions within the waters overlying Enrique reef.

	Aragonite	Calcite	5% $MgCO_3$	10% $MgCO_3$	13% $MgCO_3$	25% $MgCO_3$	30% $MgCO_3$
ΔG (cal mol^{-1} $CaCO_3$)	754	1002	858	775	699	199	-104

Biogeosciences Discuss., https://doi.org/10.5194/bg-2018-408
Manuscript under review for journal Biogeosciences
Discussion started: 12 October 2018

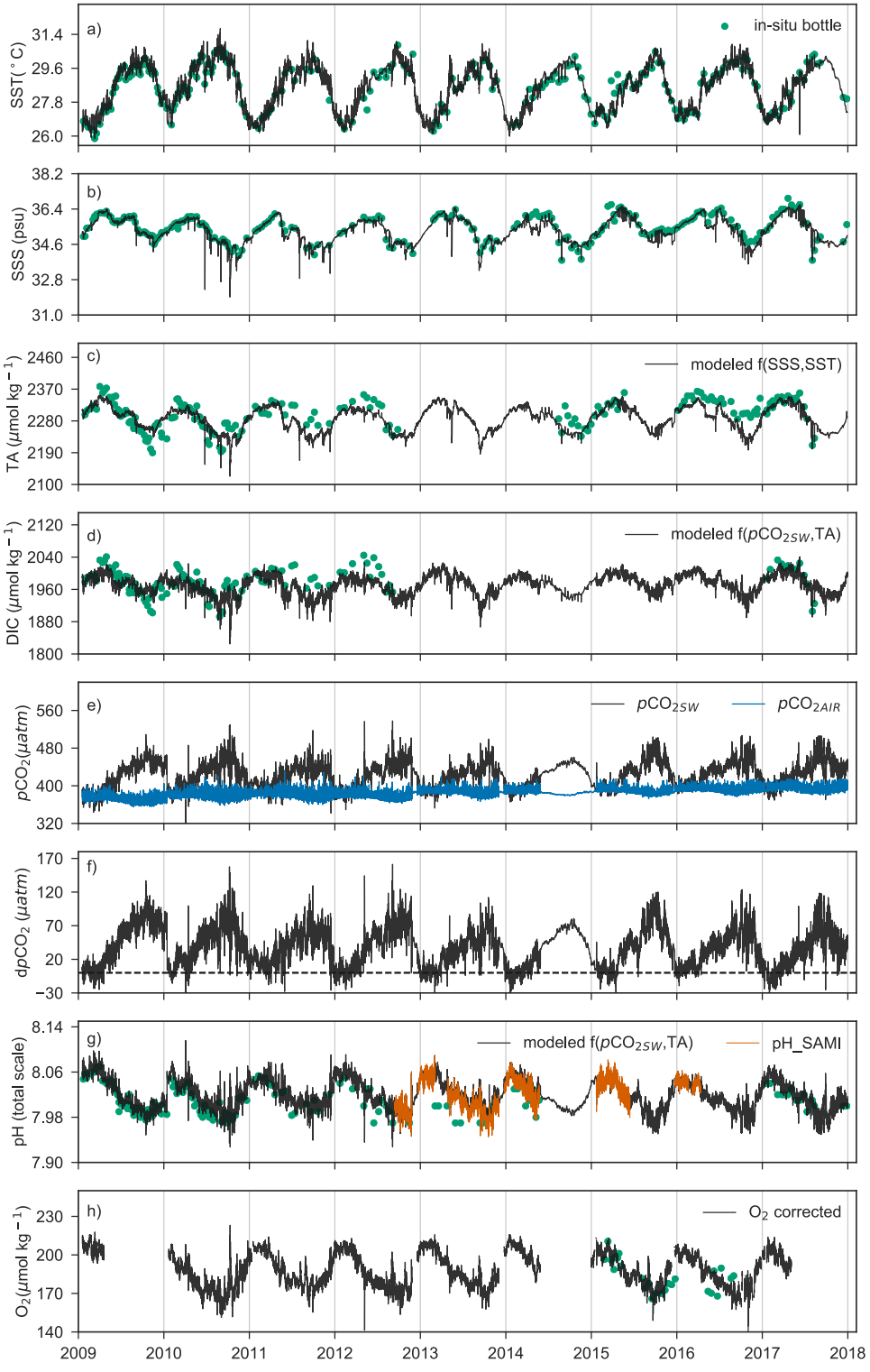

291

Biogeosciences Discuss., https://doi.org/10.5194/bg-2018-408
Manuscript under review for journal Biogeosciences
Discussion started: 12 October 2018

Figure 1: Multi-annual time series of the MapCO_2 buoy (black line) and *in situ* (green dots) geochemical measurements, and derived values from 2009 to 2017 at the forereef of Enrique reef. Final measurements used for the analyses cover from January 2009 to January 2017. The data from Feb 2017 to December 2017 is preliminary see: www.pmel.noaa.gov/co2/story/La+Parguera. Sea surface observations of: a) temperature (Temp; ^{0}C), b) salinity (Sal), c) Derived total alkalinity (TA; µmol kg^{-1}) as a function of SST and SSS (Eq.5), d) dissolved inorganic carbon (DIC; µmol kg^{-1}) as a function of pCO_2 and TA, e) seawater and boundary layer atmospheric pCO_2 ($pCO_{2,sw}$, $pCO_{2,air}$; µatm), f) air-sea gradient in pCO_2 (ΔpCO_2; µatm), g) Derived pH as a function of pCO_2 and TA and pH measurements from the SAMI-pH system (orange line), and h) Derived oxygen using the MAX-250+ sensor (O_2; µmol kg^{-1}). Data gaps filled climatological averages are highlighted in the gray shaded areas.

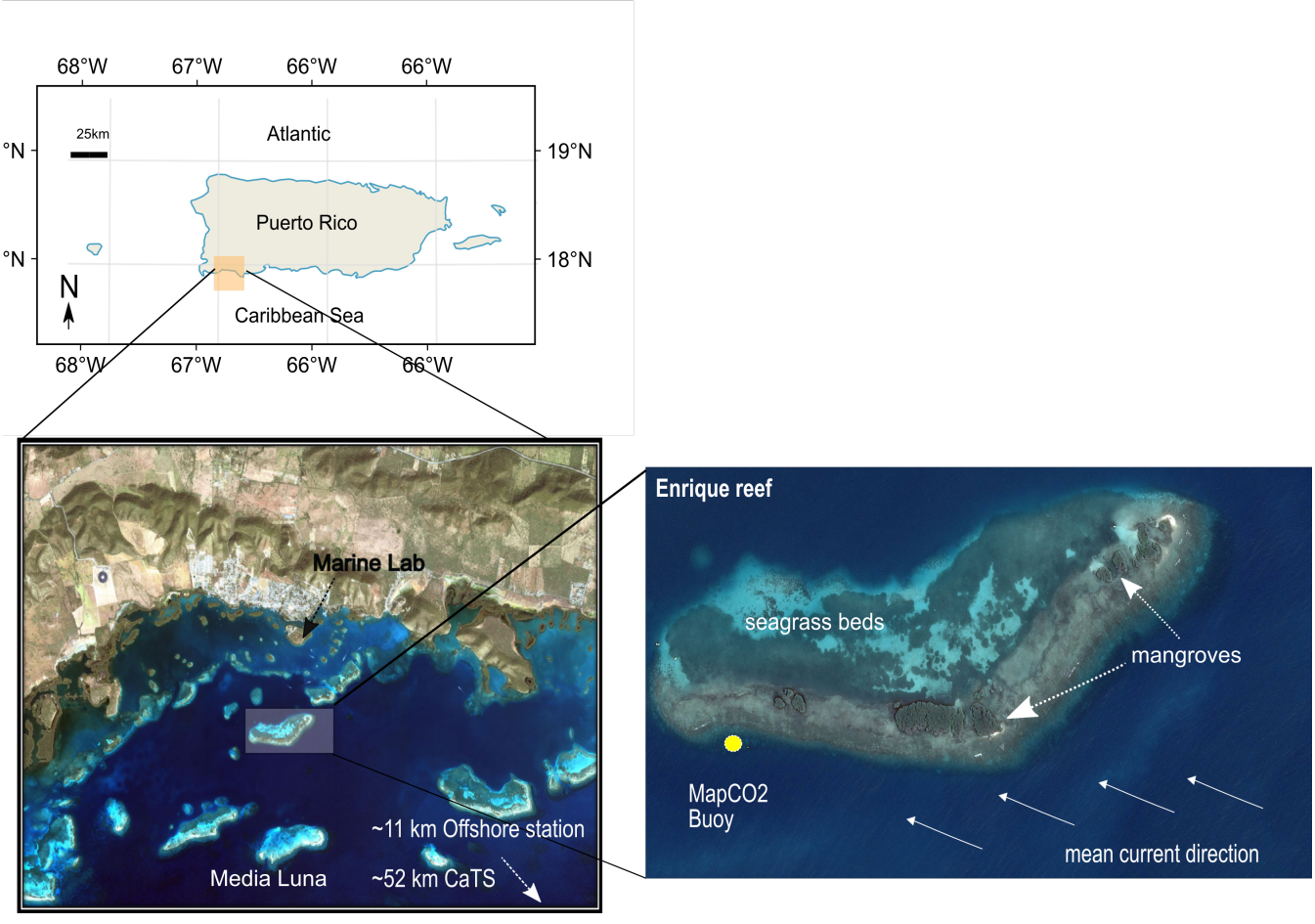

Figure 2: a) Map showing the town of Lajas (18.05° N, 67.05° W) and the Marine Protected Area of La Parguera located on the southwest coast of Puerto Rico (orange box). b) The offshore sample stations (white dashed line) include the offshore station (17.87 N, -67.02 W) located ~11 km from Enrique reef and 1.6 km south (seaward) of the shelf-edge, and the Caribbean Time Series station (CaTS, 17.36 °N, 67^0 W) at ~52 km offshore. c) The MapCO_2 buoy (17.95° N, 67.05° W) is located at the west-end of Enrique (yellow dot) and over the forereef where the water depth is ~ 3 m. Red mangroves have colonized the emergent reef island comprised by coral rubble. The dominant ocean current direction at the sea surface is towards the north-west.

Biogeosciences Discuss., https://doi.org/10.5194/bg-2018-408
Manuscript under review for journal Biogeosciences
Discussion started: 12 October 2018

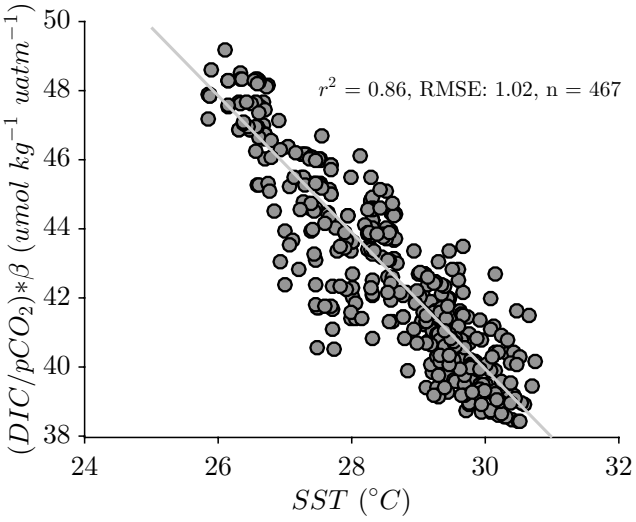

Figure 3: Linear relationship between the fractional DIC (µmol kg^{-1}) and $pCO_{2,sw}$ (µatm^{-1}) to Revelle Factor (β) and SST (ºC). This linear relationship (y = SST × -2.02 (± 0.002) + 100 (± 0.063)) was used to compute ∂DIC_{BIO} from ∂pCO_{2BIO} according to equation 11.

Biogeosciences Discuss., https://doi.org/10.5194/bg-2018-408
Manuscript under review for journal Biogeosciences
Discussion started: 12 October 2018

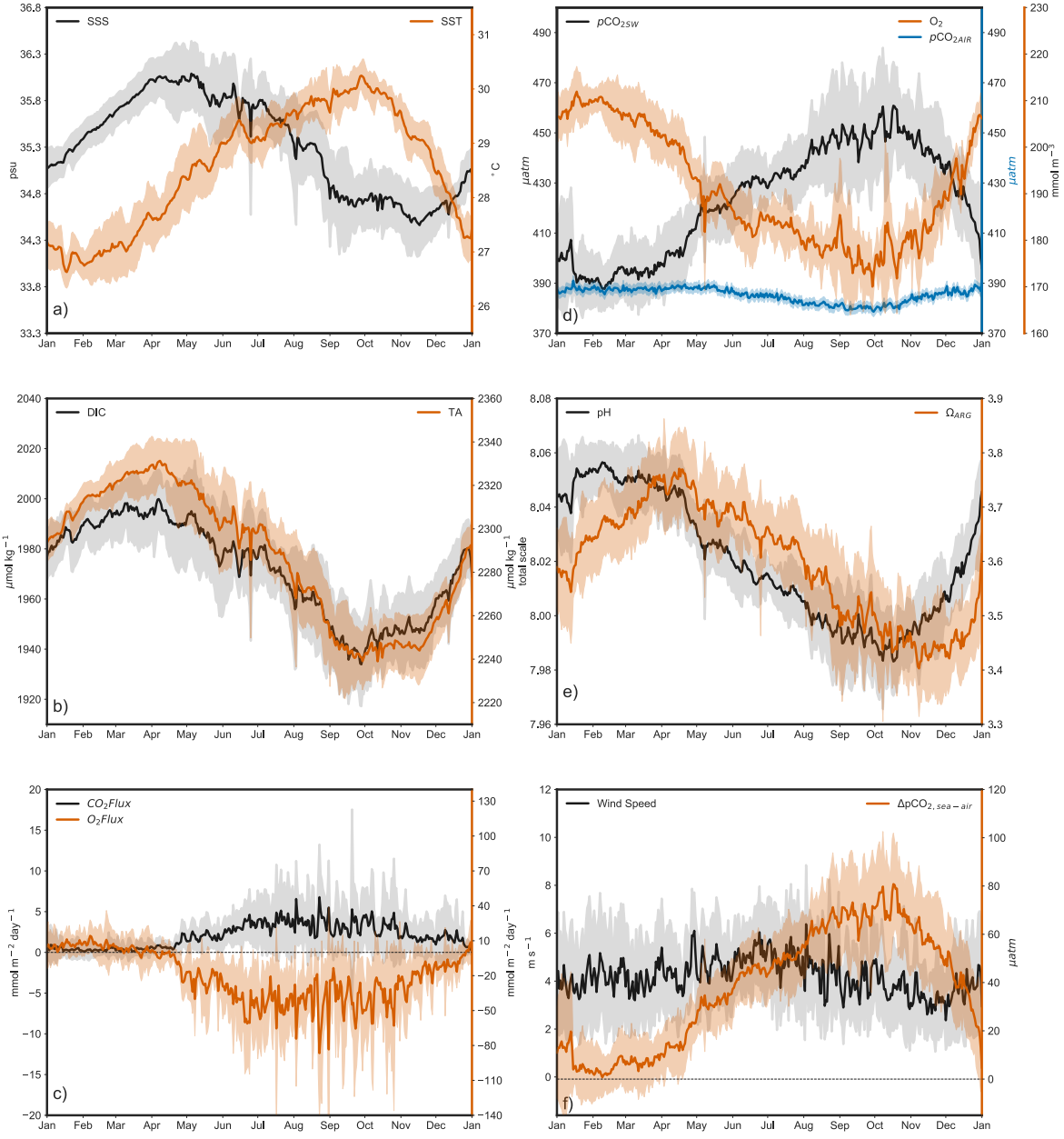

312

313 **Figure 4: Seasonal series of the buoy measurements, hydrographic properties (e.g., wind speed, fluxes) and derived carbonate**
314 **chemistry parameters (e.g., DIC, pH, Ω_{arag}). The 3-hour observations from 2009 to 2017 were binned and averaged by day. Mean**
315 **(solid line) and standard deviation (shaded bounds) demonstrate the seasonality of sea surface a) temperature (Temp; ^{0}C; orange)**
316 **and salinity (Sal; black), b) total alkalinity (TA; µmol kg^{-1}; orange) and dissolved inorganic carbon (DIC; µmol kg^{-1}; black), c) CO_2**
317 **(orange) and O_2 (black) flux (mmol m^{-2} day^{-1}), d) post-corrected oxygen from the MAX-250+ sensor (O_2; mmol m^{-2}; orange),**
318 **seawater (black) and air (blue) pCO_2 ($pCO_{2,sw}$, $pCO_{2,air}$; µatm), e) Ω_{ARG} (orange) and pH (black) and f) air-sea gradient in pCO_2**
319 **(ΔpCO_2; µatm; orange) and wind speed (m s^{-1}; black).**

Biogeosciences Discuss., https://doi.org/10.5194/bg-2018-408
Manuscript under review for journal Biogeosciences
Discussion started: 12 October 2018

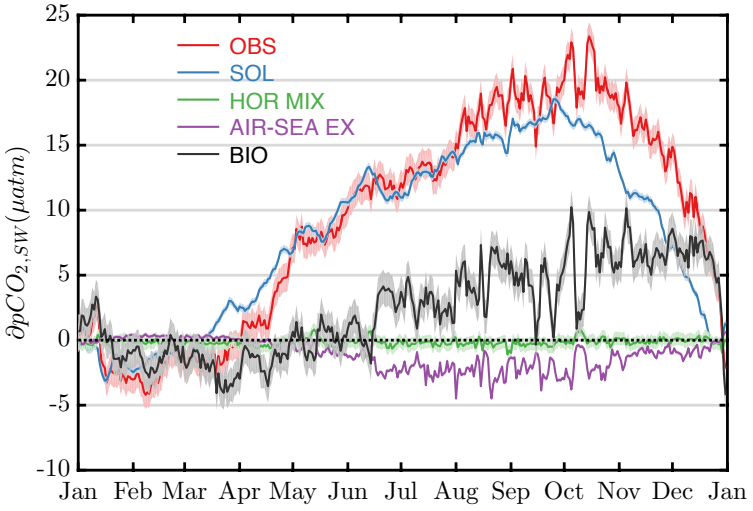

Figure 5: Cumulative seasonal change in surface $pCO_{2,sw}$ ($\delta pCO_{2,sw}$; µatm) are based on contributions from thermodynamic, physical, and biological processes at Enrique forereef. The average (solid line) is determined from 2009 to 2017 data, with model uncertainties (shaded bounds, Table 1). Observed pCO_2 values (OBS; red), effects of temperature and salinity variability (SOL; blue), effects of horizontal mixing (HOR MIX; green), effects of air-sea exchange (AIR-SEA EX; purple) and effects of biological activity (BIO; black).

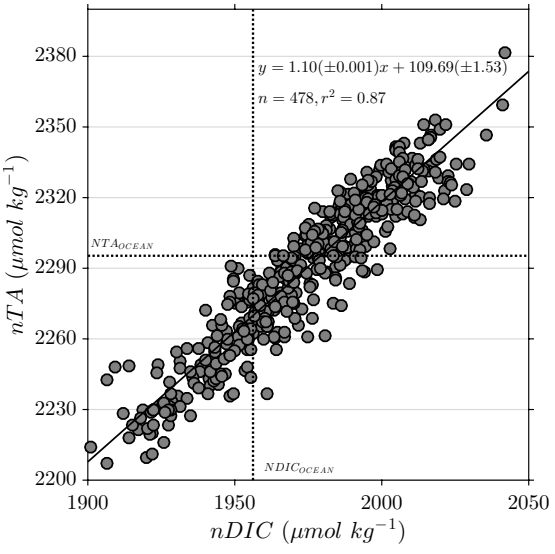

Figure 6: Relationship between salinity-normalized DIC (nDIC; µmol kg^{-1}) and salinity-normalized TA (nTA; µmol kg^{-1}) using the *in situ* bottle measurements collected at the $MapCO_2$ buoy from 2009 to 2017. DIC and TA measurements were normalized by the mean oceanic salinity (S= 36.0) to correct for the influence of freshwater addition and removal; and explore the biological processes that also influence TA and DIC.

Biogeosciences Discuss., https://doi.org/10.5194/bg-2018-408
Manuscript under review for journal Biogeosciences
Discussion started: 12 October 2018

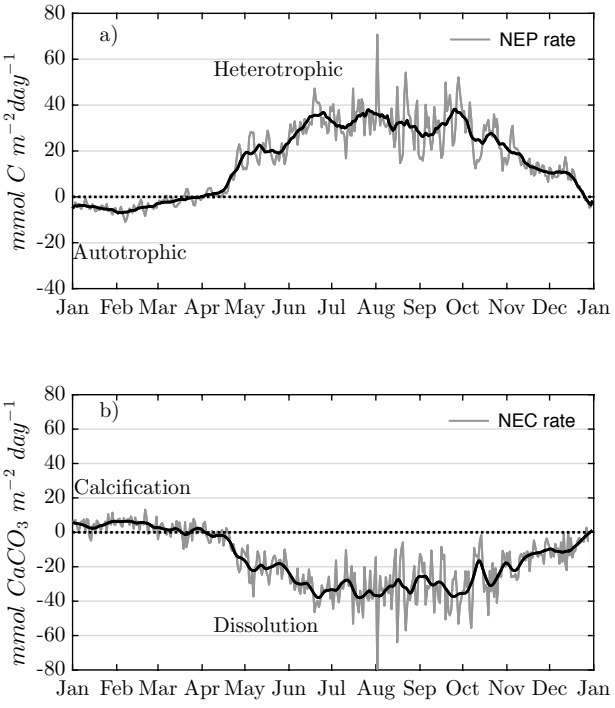

Figure 7: Annual composites based on daily averages of modeled a) NEP (mmol C m^{-2} day^{-1}; gray line) and b) NEC rates (mmol $CaCO_3$ m^{-2} day^{-1}; gray line). Solid black line is a moving average of span 15. NEP > 0 are representative of net heterotrophic and NEP < 0 indicate net autotrophic. NEC > 0 indicates net calcification and NEC < 0 net dissolution.

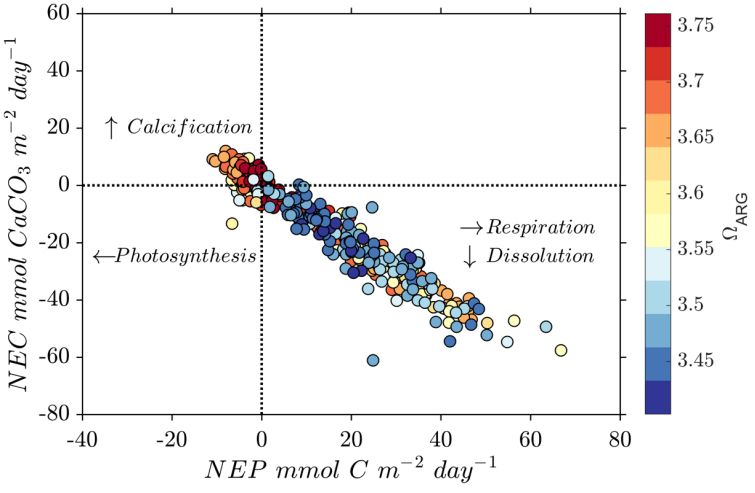

Figure 8: NEC (mmol $CaCO_3$ m^{-2} day^{-1}) versus NEP rates (mmol C m^{-2} day^{-1}) in relationship with Ω_{arag} indicated with colorbars. The zero line of NEC and NEP are denoted by grey dashed lines.

Biogeosciences Discuss., https://doi.org/10.5194/bg-2018-408
Manuscript under review for journal Biogeosciences
Discussion started: 12 October 2018

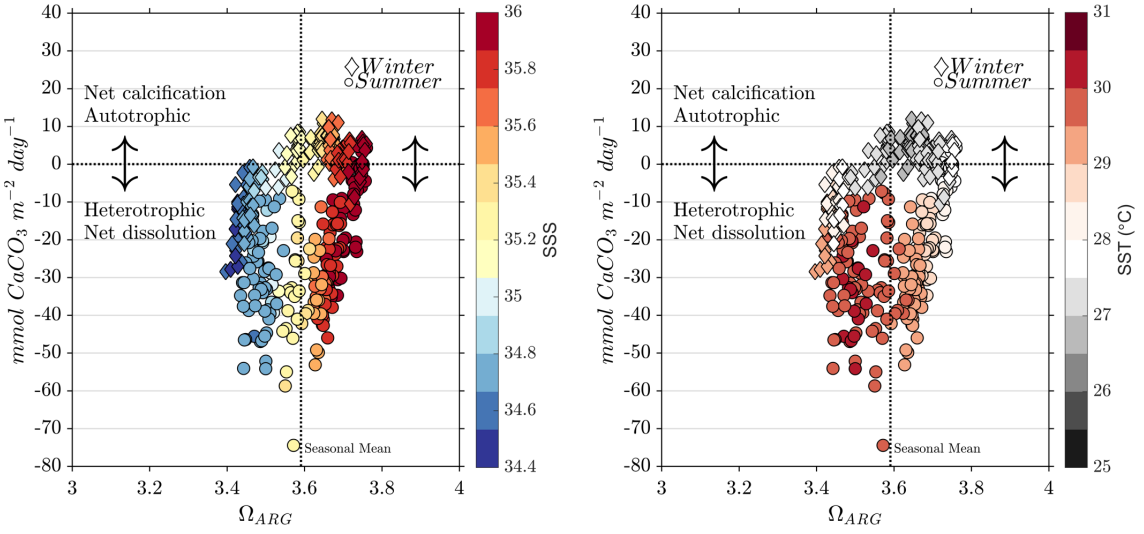

340

341 **Figure 9: Seasonal hysteresis of NEC (mmol $CaCO_3$ m^{-2} day^{-1}) relative to Ω_{arag} and colored by (a) SSS and (b) SST (°C) indicated**
342 **with colorbars. The diamond symbols represent the winter values and the circle symbols the summer. The zero line of NEC and**
343 **the seasonal mean of Ω_{arag} are denoted by grey dashed lines.**

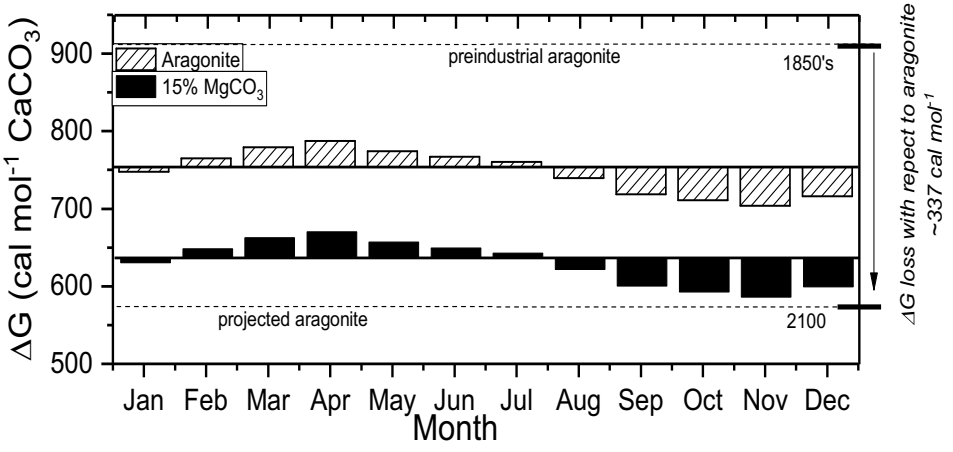

344

345 **Figure 10: Seasonal dynamics in free energy (cal mol-1 CaCO3) at Enrique reef for Aragonite (dashed) and 15% MgCO3 (solid**
346 **black). The dashed lines represent the free energy for aragonite in the 1850 and the projection for 2100.**